AN EXPERIMENTAL AND COMPUTATIONAL STUDY OF NATURAL AND HYBRID VENTILATION IN BUILDINGS

Jun Cheng

A Thesis

in

The Department

of

Building, Civil and Environmental Engineering

Presented in Partial Fulfillment of the Requirements
For the Degree of Master of Applied Science (Building Engineering) at
Concordia University
Montreal, Quebec, Canada

March 2017

CONCORDIA UNIVERSITY

School of Graduate Studies

This is to certify that this thesis is prepared

By: Jun Cheng

Entitled: An Experimental and Computational Study of Natural and Hybrid Ventilation in Buildings

and submitted in partial fulfillment of the requirements for the degree of

Master of Applied Science (Building Engineering)

complies with the regulations of the University and meets the accepted standards with respect to originality and quality.

Signed by the final examining committee:

Dr. Andreas Athientis Chair

Dr. Chevy Chen Examiner

Dr. Bruno Lee Examiner

Dr. Liangzhu (Leon) Wang Supervisor

Dr. Theodore Stathopoulos Supervisor

Approved by _____

Chair of Department or Graduate Program Director

_____ 2017 _____

Dean of Faculty

ABSTRACT

An Experimental and Computational Study of Natural and Hybrid Ventilation in Buildings

Jun Cheng

This thesis presents a few empirical formulas established by previous studies and considers their viability for more general use to determine natural ventilation airflow rates under both ventilation strategies, i.e. single-sided ventilation and cross-ventilation. By utilizing computational fluid dynamics (CFD), a series of computational simulations are conducted to determine decisive ventilation variables such as the wind incidence angle and the height of the building. Both main turbulence models, the Reynolds-averaged Navier-Stokes (RANS) two-equation standard k-ε model and the Large Eddy Simulation (LES) model are used in CFD simulations for model validation and results are compared with experimental data under steady state. The natural ventilation energy saving potentials for both ventilation strategies are determined and compared based on the empirical equations with newly developed coefficients. Additionally, such a method of evaluating natural ventilation energy saving potential can be applied during the building's early design stage as shown by a case study. Nevertheless, as a practical application of natural ventilation in a high-rise building, the hybrid ventilation system in Concordia University's EV building is studied for greater understanding and optimization of its performance. Throughout the full-scale measurements and whole-building simulations (by CONTAM), it is determined that the five-zone simplified model is accurate and helpful for further developing predictive control strategies in real buildings. A demo case study of damper opening optimization is also presented.

ACKNOWLEDGEMENT

I would like to express my sincere gratitude to my honorable supervisors Dr. Leon (Liangzhu) Wang and Dr. Theodore Stathopoulos for sharing their vast knowledge and encouraging and supporting me throughout my study and research. Thanks for giving me the opportunity to learn far beyond the textbook.

I would also like to thank my colleagues Dr. Dahai Qi, Weigang Li and Suijiang Situ for their valuable suggestions and support in my studies. Special thanks to my colleague Ali Katal who has worked so hard to adapt my VBA codes into wonderful GPU-based rendering results.

I am grateful to Dr.Jiwu Rao for generously providing the experimental equipment and teaching me how to properly use them with patience, and Daniel Gauthier from the department of Facilities Management for his advises and cooperation. I would also like to express my deep gratitude to Harry Vallianos, Sophie Yuan, Tasos Papachristou, Zisis Ioannidis and Cheng Zhang, the measurements would never be done without your generous help. It was you who made me truly understood what teamwork is. I offer my regards and respect to all professors and students in the Centre for Zero Energy Building Studies (CZEBS) for their great help and let me know the importance of communication.

I wish to recognize the support provided by the Natural Sciences and Engineering Research Council of Canada (NSERC), Dr. Duncan Phillips and Mr. Vincent Tang from RWDI Inc. for advising and generously sharing the wind tunnel experiment results.

Most importantly, I am more than grateful to my beloved family members and the ones I love for their understanding and support during my studies.

To the memory of my beloved grandfather, an ordinary but great educator.

TABLE OF CONTENTS

LIST OF FIGURES

LIST OF TABLES

NOMENCLATURE

A	area of opening, m^2
C	specific heat, J/(kg·°C)
C_1, C_2, C_3, C_μ	empirical constants of turbulence equations
C_D	discharge coefficient
C_p	pressure coefficient
dt	change in time, s
dV	change in volume, m^3
f	correction factor of single-sided ventilation
G_b	generation of turbulent kinetic energy due to buoyancy, m^2/s^3
G_k	generation of turbulent kinetic energy due to mean velocity gradients, m^2/s^3
k	turbulence kinetic energy, m^2/s^2
K	wind velocity coefficient
m	mass of air, g
P_a	local pressure of air, Pa
P_s	local static pressure, Pa
q	amount of heat, J

Q	air flow rate, m^3/s
$\overline{Q_{eff}}$	net mean air flow rate, m^3/s
Q_{in}	internal heat gain, W/m^2
S_k, S_ε	optional source terms
T_i	indoor temperature, K
T_O	outdoor temperature, K
u_i, u_j	mean velocities along coordinate axes, m/s
u'_i, u'_j	fluctuating velocities along coordinate axes, m/s
U	wind velocity, m/s
U_r	reference wind velocity, m/s
V	volume of building, m^3
x_i, x_j	distances along coordinate axes, m
Y_M	contribution of fluctuating dilatation in turbulence to overall dissipation rate
Z	height of opening, m
ΔT	temperature difference between indoor and outdoor, K

Greek letters

α	wind velocity coefficient
γ	ratio of specific heat of air
δ_{ij}	Kronecker delta
ε	turbulence dissipation energy, m^2/s^2
μ	molecular viscosity of air, m^2/s
μ_t	turbulent viscosity, m^2/s
ρ	density of air, kg/m^3
$\sigma_k, \sigma_\varepsilon$	turbulent Prandtl number of k and ε
ϕ	wind incidence angle, deg

Abbreviations and acronyms

ASHRAE	American Society of Heating, Refrigerating, and Air-Conditioning Engineers
BMS	Building Management System
CFD	Computational Fluid Dynamics
EV	Engineering, Computer Science and Visual Arts Integrated Complex
HVAC	Heating, Ventilation, and Air Conditioning
LES	Large Eddy Simulation
RANS	Reynolds-averaged Navier-Stokes
RH	Relative humidity

1 Introduction

1.1 Background

Ventilation, by definition, is the process of replacing stale or noxious air with fresh air. Furthermore, natural ventilation is the act of ventilation without the use of any mechanical forces. Building ventilation performance is directly related to the popular topic of Sick Building Syndrome (SBS). The prevalence of SBS symptoms in air-conditioned buildings is up to 200% higher than in buildings using natural ventilation [1]. Other than its improvement of indoor air quality and reduction of the risk of SBS, natural ventilation is also widely applied for its energy-saving potential. The United States Department of Energy indicates that the building sector, including residential and commercial buildings, accounts for 41% of annual energy usage, nearly half of which is consumed by space heating and cooling [2]. In Canada, this number is even higher: more than 55% of annual building energy consumption is used for space heating and cooling [3]. Specifically, it shows a total growth of 84.2% for space cooling and 1.4% for space heating in two decades according to Natural Resources Canada's Energy Use Data Handbook [4]. All the figures mentioned above indicate that the utilization of natural ventilation should be strongly considered during the early stages of building design.

Typically, there are two main types of natural ventilation: single-sided ventilation and cross-ventilation (see Figure 1.1). In single-sided ventilation, only one façade is designed to have

openings. In contrast, in cross-ventilation there are two or more openings on adjacent or opposite façades.

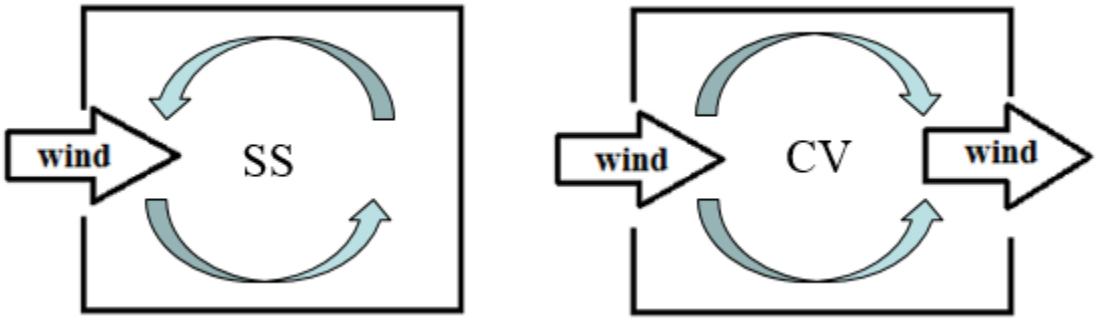

Figure 1-1. Single-sided ventilation (left) and cross-ventilation (right)

The driving forces for natural ventilation are temperature differences (buoyancy) and wind pressure differences (wind). For cross-ventilation, wind is the main driving force as long as the openings are at the same height. However, if the openings are placed at different heights, the thermal buoyancy will affect the airflow rate and either work with or against the wind depending on the location of the openings and the direction of the wind. Normally, when the ventilation is designed to be driven by thermal buoyancy (stack effect), the outlet opening is best placed on the roof in order to optimize the influence of the wind. In single-sided ventilation, the air change rate per hour (ACH) is related to the shape of the opening. Highly-placed openings are affected more greatly by thermal buoyancy than lower openings. Wider openings are affected more greatly by the wind than small and narrow openings. The size of the turbulent eddies and pulsations in the flow is also significant in single-sided ventilation.

Natural ventilation is often applied in residential buildings such as single-family houses. A two-story Danish family house located in Lystrup maximizes both cross-ventilation and the stack effect by equipping automatically controllable windows on all façades as well as the roof. With the addition of solar shading devices, the energy consumption in this house is significantly decreased [5]. The Frederick Lanchester Library at Coventry University, UK, uses tapering lightwells and perimeter stacks to enhance natural air movement throughout the building. By operating a Building Management System (BMS), the energy consumption is down to 0.049 kWh/m^2/hour which is half less than typical air-conditioned offices [6].

However, due to the difficulty of controlling airflow rates and indoor air distribution, natural ventilation throughout a building is sometimes either inadequate or inadvisable since it could decrease the comfort level of its occupants. Thus, hybrid ventilation (natural ventilation plus a mechanical fan exhaust system) is a practical choice, especially in high-rise buildings, as a solution that combines natural and mechanical forces. When natural forces do not suffice, mechanical fans can be used as a supplement to natural ventilation in order to keep building ventilation performance at an optimum and electricity consumption at an acceptable level. One of the best examples of the application of a hybrid ventilation system is in a school building in Grong, Norway. The hybrid ventilation system concept being used in this school is based on the fan-assisted natural ventilation principle [7].

1.2 Motivation

Determining the airflow rate of natural ventilation is always challenging as there are dozens of empirical equations which consider both natural ventilation strategies (single-sided and cross-ventilation) and the different driving forces (wind, buoyancy and mixed). Due to the limitations of each equation, there is no universal formula or guideline for coefficient selection that can be used for the analysis of natural ventilation potential.

In any case, as they draw advantages from both natural and mechanical forces, hybrid ventilation systems have gradually been applied for use in buildings. However, there are few on-site studies of hybrid ventilation systems in high-rise buildings. As a typical high-rise institutional building with a fan-assisted hybrid ventilation system, the Engineering, Computer Science, and Visual Arts Integrated Complex (EV building) of Concordia University is an ideal object of study for the exploration of hybrid ventilation system control strategies such as model predictive controls (MPC).

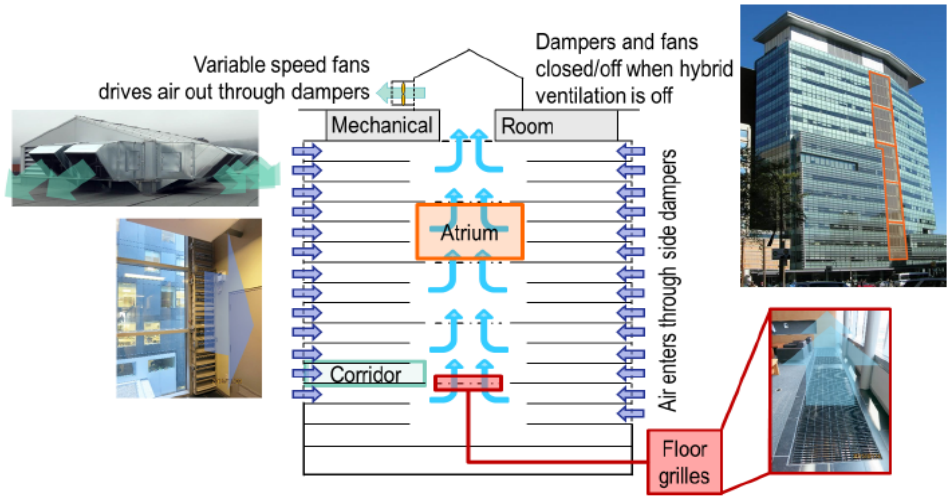

Figure 1-2. Schematic of the hybrid ventilation system in EV building [8]

1.3 Objectives

In this thesis, the main objectives are to conduct a coefficient selection for naturally ventilated buildings with a common shape through existing empirical formulas and to develop a quick and relatively accurate method of evaluating natural ventilation potential for energy-saving analysis based on such equations. A demonstrative case study would be conducted to discuss the variables. In addition, this thesis also aims at deriving a simplified and practical model for system optimization study and implementing MPC that can be calibrated in a real high-rise building (EV building) with a hybrid ventilation system. Moreover, this model must support further development in order to integrate energy balance calculations for thermal mass analysis for MPC applications of building thermal storage in the next research stage.

1.4 Approaches of the research

By reviewing the existing empirical models for calculating natural ventilation airflow rate, two representative wind-driven models for two different ventilation strategies were selected and combined with a set of computational fluid dynamics (CFD) simulations to generate the coefficient selection guideline. Excel-VBA was used to develop a method of evaluating natural ventilation energy-saving potential which takes into consideration building terrain, window type, window-to-wall ratio, etc. Nonetheless, through a series of on-site measurements in the EV building under different weather conditions and different conditions of fan operation, a calibrated, simplified dynamic model was created in CONTAM to carry out full-building simulations in order to optimize the performance of the hybrid ventilation system.

1.5 Thesis outline

Chapter 1 introduces the general concepts, driving forces and strategies of natural ventilation, the importance of using natural ventilation to save energy and one of the practical applications of natural ventilation in high-rise buildings, i.e., hybrid ventilation.

Chapter 2 provides a literature review including existing empirical equations for the calculation of the airflow rate of natural ventilation, an overview of the EV building and related studies and a review of exemplary existing buildings with different ventilation strategies.

Chapter 3 presents the study of natural ventilation in building early design stage, including determining the value of coefficients, proposing a method of evaluating natural ventilation potential, followed by energy saving analysis and a case study.

Chapter 4 describes the study of hybrid ventilation in a high-rise building for predictive control based on full-scale measurements and whole-building simulation. A demo study is included to discuss the optimization of hybrid ventilation performance.

Chapter 5 summarizes the research conclusions and suggests future work.

2 Literature Review

This chapter firstly determines the key parameters which can quantify and qualify ventilation performance, then provides a review of a series of existing empirical formulas for natural ventilation under different scenarios. It also provides an overview of the EV building's hybrid ventilation system and related studies. A review of exemplary existing buildings with different ventilation methods follows.

2.1 Key parameters to quantify and qualify ventilation performance

When determining the natural ventilation airflow through openings, there are many key parameters such as outdoor weather conditions (outdoor temperature and wind characteristics), opening details and thermal comfort which can make a difference.

2.1.1 Outdoor weather conditions

As mentioned previously, the driving forces of natural ventilation are temperature and wind. Thus, the outdoor weather conditions are key to the study of everything related to natural ventilation.

Historical weather data are often used in modeling, prediction and simulation [9], [10]. For building simulations carried out under Canadian and North American conditions, typical weather data sets like TMY (Typical Meteorological Year) and CWEC (Canadian Weather for Energy Calculations) were commonly used [11], [12]. The TMY files were created by the U.S Department of Energy's (DOE) National Renewable Energy Laboratory (NREL) in 1981 and derived from records dating from 1948 to 1980. Each file contains a set of hourly data concerning solar radiation and meteorological elements for a 1-year period from a specific weather station. Similarly, the

CWEC files include hourly weather records representing an artificial 1-year period specifically designed for building energy calculations. These files are produced by Numerical Logics in collaboration with Environment Canada and the National Research Council of Canada [13]. However, it is recommended that building simulation users regularly use more than one weather file to capture a range of building performance [14].

Wind characteristics play an important role in terms of the calculation of natural ventilation air flow. The amount of air coming through the openings depends highly on the outdoor wind velocity and direction, especially in wind-driven single-sided natural ventilation where the pulsating flows dominate the air exchange [15].

Since wind velocity data is often measured in large open spaces like airports, a correction is thus needed for wind in other locations such as urban areas. A universal expression can be applied to do so:

$$U = U_r \times K \times Z^{\alpha} \qquad \text{Eq. 2-1}$$

where the coefficients K and α depend on the terrain as shown in following table:

Table 2-1. Wind velocity coefficients K and α under different terrain [16]

Terrain	$\boldsymbol{K}$	$\boldsymbol{\alpha}$
Open flat countryside	0.68	0.17
Countryside with scattered wind breaks	0.52	0.20
Suburban area	0.35	0.25
Urban area	0.21	0.33

2.1.2 Opening type

Karava et al. [17] points many aspects of openings can affect the airflow, such as the window-to-wall ratio, inlet-to-outlet ratio, and location, etc. Specifically, the airflow through openings varies considerably when different discharge coefficient C_D values are used [18]. In Wang et al. [19], factors like window area, height-width ratio, the opening rate of the windows and the temperature difference between the inside and outside of the windows are discussed regarding three different types of windows: (see Figure 2-1).

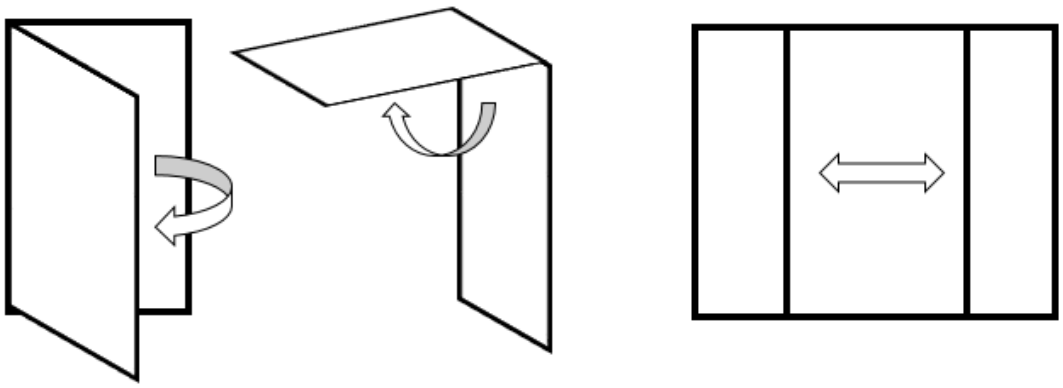

Figure 2-1. Typical types of window, side-hung window (left), hung window (middle) and sliding window (right)

Figure 2-2 shows the relation between the discharge coefficient C_D and the area of windows. It shows that when the window height-width ratio is 1, all windows are fully opened and the temperature difference between the inside and outside of the window is 0 °C, the average C_D is 0.65, 0.55 and 0.35 for side-hung window, hung window and sliding window respectively where the window area varies from 1 m^2 to 5 m^2.

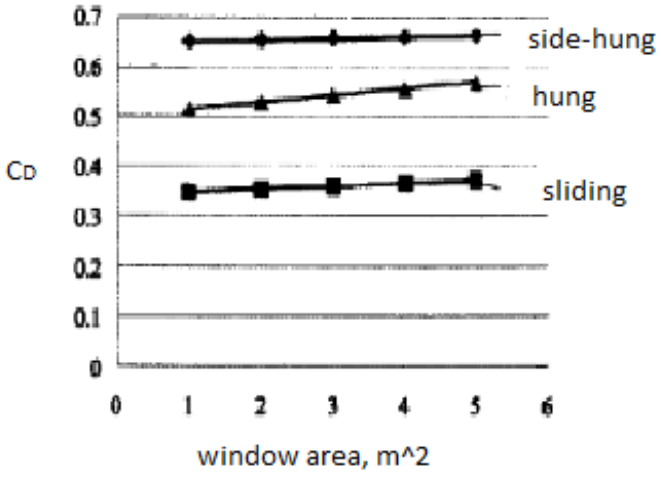

Figure 2-2. The relation between CD and window area [19]

Besides the parameters mentioned previously, Karava et al. [20] also supplements the wind angle and Reynolds number as variations of the discharge coefficient C_D as well. It also points out that using constant C_D might be one of the source of error since significant difference was found by comparing previous studies, especially in wind-driven cross ventilation.

2.1.3 Thermal comfort

When building occupants are not satisfied with their thermal environment, not only does it affect their ability to function effectively, it can also lead to health issues. Thermal comfort (TC) is achieved by a combination of many factors:

- Air temperature – both ambient air temperature and mean radiant temperature
- Relative humidity
- Relative air velocity
- Basic clothing insulation
- Metabolic energy production

The 2013 ASHRAE Handbook: Fundamentals [21] recommends comfort zones (see Figure 2-7) in both summer and winter with acceptable ranges of operative temperature and humidity with air speed less than 0.2m/s for people wearing 1.0 and 0.5 clo clothing during primarily sedentary activity which is less than 1.1 met.

However, a simplified linear regression model derived by Brager et al. [22] shows the relationship between the mean thermal sensation (TS) and the mean indoor operative temperature (T_{op}) in order to judge the thermal comfort of occupants in naturally ventilated buildings:

$$TS = 0.27 \times T_{op} - 6.65 \left(T_{op}\ in\ ℃\right)$$

Eq. 2-2

In Eq.2-2, TS represents a vote on the familiar ASHRAE seven-point thermal sensation scale, where TS=0 means neutral, TS=+3 means hot and TS=-3 is cold. Traditionally, a "neutral thermal sensation" is assumed to be the ideal condition. This equation was conducted based on 36 out of 44 naturally ventilated office buildings with almost 8900 subjective votes. The selected buildings were located on four continents and covered seven climate zones [23], [24]. However, through field studies, it was found that Eq.2-1 had overestimated the TC perception for warmer regions and resulted in a lower neutral temperature (when TS=0) [25]–[27]. Nonetheless, Eq.1 is still suggested for universal application in natural ventilation buildings regardless of the climatic conditions due to its simplicity [25].

2.2 Empirical models for single-sided natural ventilation

Since the turbulence in the wind and the variation in the pressure differences play significant roles in single-sided ventilation, thus, unlike the calculation of cross-ventilation, it is not reasonable just

to look at the average wind velocity and pressure difference when it comes to calculate the airflow rate in the case of single-sided ventilation. Moreover, because of the instability of these factors, it would be much harder to calculate accurately. However, in recent decades, more and more empirical expressions were found from full-scale outdoor experiments and/or wind tunnel experiments. These equations are classified into three main groups: wind-driven, thermal buoyancy-driven and a combination of wind and thermal buoyancy.

2.2.1 Airflows driven by wind

As emphasized, turbulence and fluctuations in the wind significantly affect the airflow rate in cases of single-sided natural ventilation. In Warren's early study [28], the dependence of the local wind velocity in front of the opening (U_L) and a reference velocity (U_R) on the incidence angle of the wind were considered.

The expressions found which originated from theoretical considerations of both wind tunnel and full-scale experiments were improved in [29].

The wind tunnel tests are described as follows:

- The box was 0.5 x 0.5 x 0.5 m and the side faced towards the wind tunnel.
- It was only possible to test wind directions parallel to the following type of openings.
    - Square openings;
    - Slot openings (longest dimension perpendicular to the flow direction and equal to the box height);
    - Single opening with vane. Three models of casement windows with different aspect ratios (1.0, 1.6 and 2.5) were tested with four different opening angles (0°, 30°, 60°

and 90°), three directions of the flow (0° 90° and 180°) and up to six different velocities in the tunnel;

- Two openings with vane.

Two full-scale experiments were carried out in two different buildings (one was a single-story building, another was a three-story school building) to compare with theoretical and experimental data. From all the experiments described, two equations are derived without the influence of temperature difference, in addition, it is noted that the combinations of window shapes, certain wind directions and high-rise building might lead to higher ventilation flow rates:

$$Q_{\mathrm{v}} = 0.1 \times \mathrm{A} \times \mathrm{U_L} \qquad \text{Eq. 2-3}$$

$$Q_{\mathrm{v}} = 0.025 \times \mathrm{A} \times \mathrm{U_R} \qquad \text{Eq. 2-4}$$

It is noted that the numbers 0.1 and 0.025 are flow numbers from experiments. L stands for local, T stands for top of building and R stands for reference velocity (in Eq. 2-4) this reference velocity was measured at the height of 10 m.

Crommelin et al. [30] also proposed few correlation methods for wind-driven single-sided ventilation calculations. Specifically, a correlation between the airflow and the standard deviation of pressure, the velocity and the area of the opening was found via a wind tunnel experiment. As the results, it can be found that increasing wind speed results in a growing volume of airflow through the opening, because the shorter upstream length has a higher turbulence in the flow, meaning there is an increase in the fluctuating airflow. Therefore, an obvious difference in the airflow depending on the upstream length towards the fan was observed.

The final expressions are as follows:

$$\sigma_{\Delta P} = \alpha_1 \times U^2 \quad \text{Eq. 2-5}$$

$$Q = \alpha_2 \times (\sigma_{\Delta P})^{\beta_1} = (\alpha_1)^{\beta_1} \times \alpha_2 \times U^{2\beta_1} \quad \text{Eq. 2-6}$$

$$Q = \alpha_3 \times A^{\beta_3} \quad \text{Eq. 2-7}$$

where:

$\sigma_{\Delta P}$ is the standard deviation of pressure (m/s)

α is the empirical coefficient

β is the empirical coefficient

For an upstream length of 0.35 m, $\alpha_1 = 0.029$, $\alpha_2 = 0.0018$, $\alpha_3 = 0.0608$, $\beta_1 = 0.32$, $\beta_3 = 0.92$.

By reviewing Wang, H et al. [31], a new empirical model was developed to predict the mean ventilation rate and fluctuating ventilation rate due to the pulsating flow and eddy penetration of single-sided, wind-driven natural ventilation in buildings.

The empirical models are as following:

- Ventilation rate due to mean airflow as:

$$Q = \frac{C_d l \sqrt{C_P} \int_{z_o}^{h} \sqrt{z^{\frac{2}{7}} - z_o^{\frac{2}{7}}}\, dz}{z_{ref}^{1/7}} U \quad \text{Eq. 2-8}$$

- Fluctuating ventilation rate contributed by pulsating flow as:

$$\sigma_{q_p}^2 = \left(C_d l \frac{1}{z_{ref}^{1/7}} \sqrt{C_P} \int_{z_0}^{h} \sqrt{z^{2/7} - z_0^{2/7}}\, dz \right) \sigma_u^2$$

Eq. 2-9

- Fluctuating ventilation rate due to eddy penetration as:

$$\sigma_{q_e}^2 = C^2 A^2 \overline{U} \int_{\overline{U}/l}^{\infty} S(\tilde{n}) d\tilde{n}$$

Eq. 2-10

where: l = opening width, z_0 = position of the neutral plane, S = power spectrum.

In Cockroft et al. [32], the air change rate was analyzed for a single-sided ventilation driven by wind only. A mathematical pulsation model was derived from a single opening pulsation flow. The expression was also examined via a wind tunnel experiment on a wooden box of 1.2 x 1.2 x 2.4 m with a single opening of 15.2 cm^2.

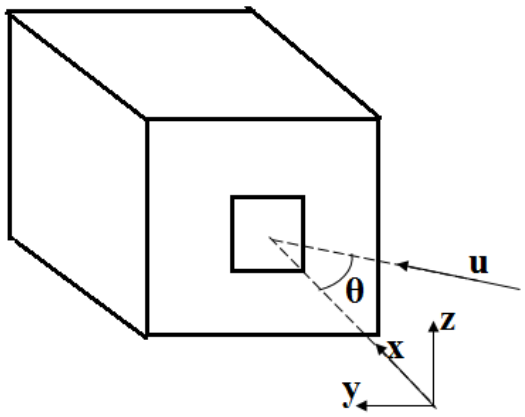

Figure 2-3. Coordinated representation of the expression (after Cockroft et al. [32], modified)

$$q = \frac{dv}{dt} = \pm C_D \times A \times \sqrt{\left| {u_{x,a}}^2 - \left(\frac{2\gamma P_a}{\rho V}\right) * v \right|}$$

Eq. 2-11

$$\overline{q_{eff}} = \frac{1}{2} \times f \times q$$

Eq. 2-12

where:

q is the air flow rate (m^3/s)

$\overline{q_{eff}}$ is the net mean effective flow rate (m^3/s)

f is the correction factor between 0 to 1 for how thoroughly the inflow air mixed with the inside air

dV is the change in volume (m^3)

γ is the ratio of specific heat of air, 1.4 for adiabatic flows and 1.0 for isothermal flows

C_D is the discharge pressure coefficient equals 0.65 in this case

Pa is the pressure of air (Pa)

ρ is the density of air (kg/ m^3)

$u_{x,a}$ is the wind velocity in x direction (m/s)

As shown in Eq.2-20, the effective ventilation rate $\overline{q_{eff}}$ is defined as the ratio f multiplied by the air going into the space. It was found that 37% of the airflow rate contributed to the effective air change by using the tracer gas decay method [32].

As with the others, this model has some limits and assumptions:

- Wind turbulence is disregarded since only low frequency airflow is driven in this model;
- The flow is quasi-steady, and the stagnation pressure of the airstream is generated immediately outside the opening;
- The opening behaves as a sharp orifice;
- The Reynolds's number is high enough for Bernoulli's theorem to apply;
- Internal pressure is assumed to be a constant;
- The enclosure is assumed to be an adiabatic system.

2.2.2 Airflows driven by buoyancy

Buoyancy force is another main factor to drive outdoor air coming into building through openings and/or indoor air moving from the bottom to the top of building (i.e. stack effect). Before any approaches were proposed, researchers assumed the indoor air temperature was constant; indoor temperature stratification and varying air density were neglected.

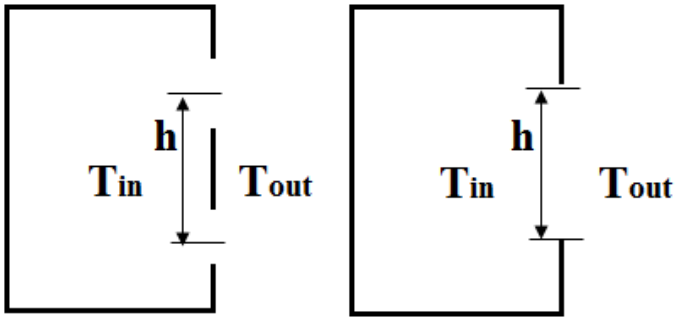

Figure 2-4. Flow through an upper and a lower opening (left) and flow through a single opening (right) (after Warren et al. [29], modified)

From Warren et al. [29], two expressions were applied for airflow calculation. Firstly, for single-sided ventilation through upper and lower openings of equal area, A, the volume flow rate through each one is about:

$$\dot{V} = C_D A \sqrt{gh\frac{\Delta T}{T_{out}}}$$

Eq. 2-13

Where h is the distance between the center of two openings, C_D is equal to 0.6 for the doorway. As this literature mentions, this equation is valid when the difference between the outside and the average inside temperature ΔT is less than 10°C.

Another equation was used to calculate the volume flow rate through a single large opening:

$$\dot{V} = \frac{C_D A}{3} \sqrt{gh\frac{\Delta T}{T_{out}}}$$

Eq. 2-14

where h is the height of the window.

2.2.3 Airflows driven by wind and buoyancy

As a result of de Gids and Phaff's method [33], a general expression is proposed for the ventilation rate Q through an open window as a function of temperature difference, wind velocity and fluctuating terms. In the case of single-sided ventilation, the effective velocity U_{eff} is defined as the flow through half of a window opening:

$$U_{eff} = \frac{Q}{\frac{A}{2}} = \sqrt{\left[\frac{2}{\mathrm{g}} \times (\Delta \mathrm{P}wind + \Delta \mathrm{P}stack + \Delta \mathrm{P}turb)\right]}$$

Eq. 2-15

Leading to the form:

$$U_{eff} = \frac{Q}{\frac{A}{2}} = \sqrt{(C1U_r^2 + C2H\Delta T + C3)}$$

Eq. 2-16

where:

U_r = reference wind velocity, m/s

H = vertical size of the opening, m

C1 = 0.001, a dimensionless coefficient depending on the wind

C2 = 0.0035, a boundary constant,

C3 = 0.01, a turbulence constant.

Thus, to calculate the airflow rates driven by both wind and buoyancy, the expression could be written as:

$$Q = \frac{A}{2} \times U_{eff} = \frac{A}{2} \times \sqrt{(0.001U_r^2 + 0.0035H\Delta T + 0.01)}$$

Eq. 2-17

According to Larsen [15], a series of wind tunnel experiments in a full-scale building were conducted at the Japanese Building Research Institute (BRI) in 2002. The details about this experiment are listed below:

- The wind speed in the tunnel could be varied between 1 and 5 m/s with a turbulence intensity of less than 5%.

- The test building was made as a full-scale model sized 5.56 x 5.56 x 3 m, (wall thickness =0.1m)
- The room volume used in the calculations is 68.95 m^3.
- During the experiments, the model was rotated between 0° and 345°

After many wind tunnel and outdoor experiments were conducted, a new design expression for single-sided ventilation was found by Larsen [15] that included the shape of the building and the incidence angle of the wind by comparing the experimental results with previous studies.

The new design expression is shown as Eq.2-18.

$$Q = \sqrt{C_1|C_P|U_r^2 + C_2 h\Delta T + C_3 \frac{\Delta C_{P,opening}\Delta T}{U_r^2}}$$

Eq. 2-18

where the constants C1, C2 and C3 are defined as Table 2-4:

Table 2-2. Constants C1, C2 and C3 under different scenarios

	C1	C2	C3
Windward	0.0012	0.0006	-0.0006
Leeward	0.0026	0.0006	0.0273
Parallel	0.0012	0.0004	0.0097

and $\Delta C_{p,opening}$ is calculated from：

$$\Delta Cp, opening = 9.1894 \times 10 - 9 \times \varphi 3 - 2.626 \cdot 10 - 6 \times \varphi 2 - 0.0002354 \times \varphi + 0.113$$

Eq. 2-19

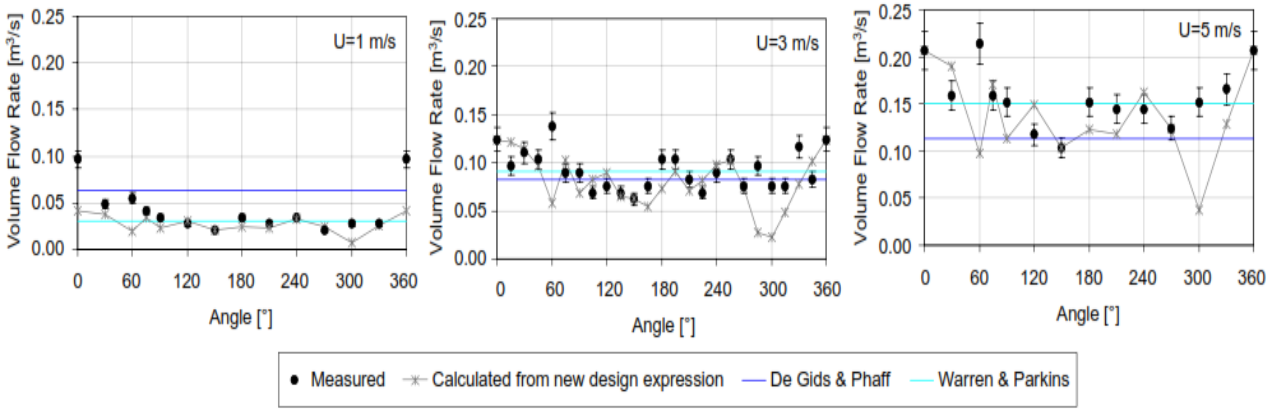

Figure 2-5. Comparison between measured and calculated results when ΔT = 0 °C [15], [29], [33]

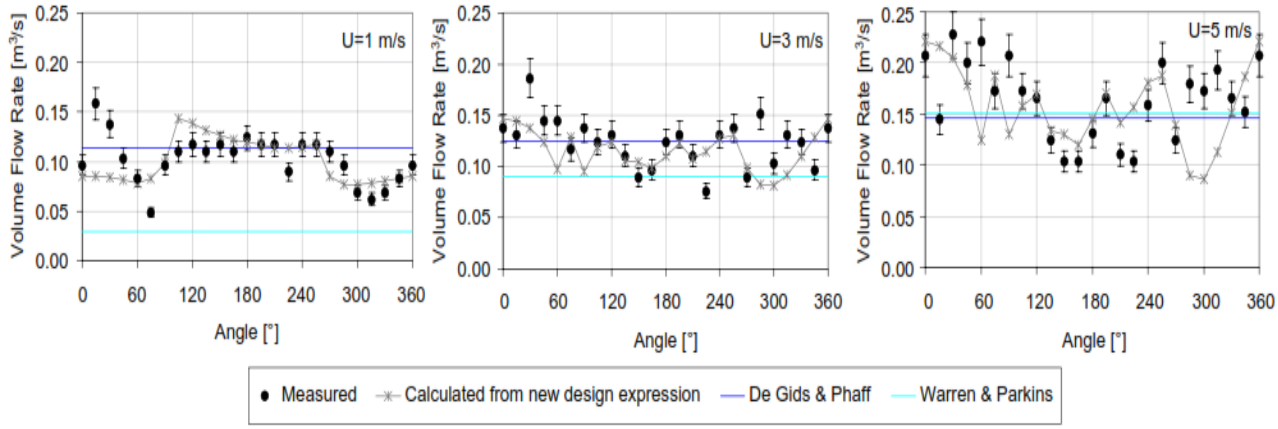

Figure 2-6. Comparison between measured and calculated results when ΔT = 5 °C [15], [29], [33]

2.3 Empirical models for cross natural ventilation

Cross-ventilation has been studied by many researchers due to its widespread use and conciseness in comparison with single-sided ventilation. Similar to previous section, this section introduces airflows driven by either wind, thermal buoyancy or a combination of the two.

2.3.1 Airflows driven by wind

Allard et al. [34] introduced the British Standard method which wind-driven, cross natural ventilation is included, and this method assumes two-directional flow through a building and ignores all internal partitions.

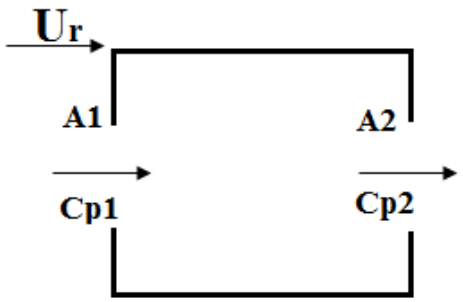

Figure 2-7. Cross ventilation with two opposite openings

The expression is shown below:

$$Q = \sqrt{\frac{Cp_1 - Cp_2}{\frac{1}{A_1^2 * C_{D_1}^2} + \frac{1}{A_2^2 * C_{D_2}^2}}} \cdot U_r \qquad \text{Eq. 2-20}$$

where:

U_r = velocity at reference height, m/s

C_D = discharge coefficient

C_p = pressure coefficient

A = opening area, m^2

2.3.2 Airflows driven by buoyancy

In order for airflow to be induced by thermal buoyancy, openings must be situated at different heights in the building. However, it does not matter whether the openings are located in different walls of the building. This section is thus also valid for single-sided ventilation with more than one opening.

The pressure difference generated by thermal buoyancy and a general method to calculate airflow can be derived as Etheridge et al. proposed [35]:

$$\Delta P_{buoyancy} = \rho_e \times g \times (H_0 - H_1) \times \frac{T_i - Te}{T_i}$$

Eq. 2-21

$$Q_v = \mp C_D \times A \times \sqrt{\frac{2 * |\Delta P|}{\rho}}$$

Eq. 2-22

If $\Delta P_{buoyancy}$ is substituted into Q_v, the airflow rate induced by thermal buoyancy through one opening can be written as seen in Eq.2-23:

$$Q_v = \mp C_D \times A \times \sqrt{\frac{2 \times \left|\rho_e \times g \times (H_0 - H_1) \times \frac{T_i - Te}{T_i} \Delta P\right|}{\rho}}$$

Eq. 2-23

where: H_0 = the height of neutral plane,

H_1 = the height below the neutral plane.

2.3.3 Airflows driven by wind and buoyancy

Most often, the airflow in natural ventilation is produced by a combination of wind and thermal buoyancy. In such situations, the pressure differences derived from Eq. 2-20 and Eq. 2-23 are combined to summarize the resultant pressure difference and thereby also the airflow [36].

$$\mathrm{Q_v} = {}^1\!/_2 \sum_{j=1}^{n} C_{D,j} \cdot A_j \cdot \sqrt{\frac{\left| {}^1\!/_2 \, C_{p,j} \rho_\mathrm{e} U_r^2 - P_i + \frac{\rho_e \Delta T}{\mathrm{T_i}} \mathrm{g}(\mathrm{H_0} - \mathrm{H_j}) \right|}{{}^1\!/_2 \, \rho_j}}$$

Eq. 2-24

It is noted that the neutral plane is found from mass balance, C_D is the same for each different opening and the internal pressure is found from an iterative solution of the mass balance.

2.4 Existing empirical models of airflow rates estimation summary

Table 2-3. Existing empirical models of airflow rate estimation. SS=single-sided ventilation, CV=cross-ventilation, W=wind-driven, B=buoyancy-driven, W&B=wind- and buoyancy-driven

Configuration	Equation	Reference
SS, W	$Q_v = 0.1AU_L$ $Q_v = 0.025AU_R$ where U_L= local wind velocity in front of opening U_R= reference wind velocity	wind tunnel tests and full-scale experiments in two real buildings by Warren at al. [29]
SS, W	$Q = \frac{dv}{dt} = \pm C_D \cdot A \cdot \sqrt{\left\lvert U^2 - \left(\frac{2 \cdot \gamma \cdot P_a}{\rho \cdot V}\right) \cdot v \right\rvert}$ $\overline{Q_{eff}} = \frac{1}{2} \cdot f \cdot Q$	pulsation model derived from wind tunnel experiment by Cockroft et al. [32]
SS, W	$Q = (\alpha_1)^{\beta_1} \cdot \alpha_2 \cdot U^{2\beta_1}$ $Q = \alpha_3 \cdot A^{\beta_3}$ where $\alpha_1 = 0.029$, $\alpha_2 = 0.0018$, $\alpha_3 = 0.0608$, $\beta_1 = 0.32$, $\beta_3 = 0.92$ for an upstream length of 0.35 m	wind tunnel experiment by Crommelin [30]

SS, W	$Q = \frac{C_D l\sqrt{C_P}\int_{z_o}^{h}\sqrt{z^{\frac{2}{7}} - z_o^{\frac{2}{7}}}\,dz}{z_{ref}^{1/7}}U$	pulsation flow derived from CFD large eddy simulation by Wang et al. [31]
SS, B	$Q = \frac{C_D A}{3}\sqrt{gh\frac{\Delta T}{T_{out}}}$	semi-analytical model by Allocca et al. [37]
SS, W&B	$Q = \frac{A}{2}\times\sqrt{\left(0.001U_r^2 + 0.0035H\Delta T + 0.01\right)}$	theoretical expression and full-scale experiments by de Gids et al. [33]
SS, W&B	$Q = \sqrt{C_1\lvert C_P\rvert U_r^2 + C_2 h\Delta T + C_3\frac{\Delta C_{P,opening}\Delta T}{U_r^2}}$	wind tunnel test and full-scale measurements on real buildings by Larsen [15]
CV, W	$\mathrm{Q} = \sqrt{\frac{\mathrm{Cp_1} - \mathrm{Cp_2}}{\frac{1}{\mathrm{A_1^2 * C_{D_1}^2}} + \frac{1}{\mathrm{A_2^2 * C_{D_2}^2}}}}\cdot \mathrm{U_r}$	The British Standards introduced by Allard et al. [34]
CV, B	$\mathrm{Q_v} = \mp \mathrm{C_D}\cdot \mathrm{A}\cdot\sqrt{\frac{2\times\left\lvert \rho_e \times g \times (H_0 - H_1)\times\frac{T_i - Te}{T_i}\Delta P\right\rvert}{\rho}}$	multiple openings model derived by Etheridge [38]
CV, W&B	$\mathrm{Q_v} = {}^1\!/_2\sum_{j=1}^{n} C_{D,j}\cdot A_j\cdot\sqrt{\frac{\left\lvert {}^1\!/_2\, C_{p,j}\rho_e U_r^2 - P_i + \frac{\rho_e \Delta T}{T_i} g(H_0 - H_j)\right\rvert}{{}^1\!/_2\,\rho_j}}$	combined model derived by Heiselberg [36]

Another interest of this section is to explore the difference between existing empirical equations. As can be found from the table above, there are four different expressions for wind-driven, single-sided natural ventilation airflow rate. Specifically, in Warren's expression and Crommelin's expression, besides the opening area A and wind velocity U, the rest of parameters are constants which directly come from experimental results to specific models. In Cockroft's equation, since the discharge coefficient C_D could be represented by constant empirical value. Thus, there is actually only one unknown f needs to be determined. However, in Wang's equation, besides the wind pressure coefficient C_P, the existence of another unknown would complicate the problem. Because the determination of the height of neutral plane z_0 depends on many other unknown

parameters. Therefore, for purpose of generalization and simplification, only the equations with one unknown would be selected for further study in this research.

2.5 Review of exemplary existing buildings with various ventilative technologies

Since natural and/or hybrid ventilation has already been widely applied in buildings around the world, it is worth reviewing some representative existing buildings with different ventilation methods. The Executive Committee of the International Energy Agency's Energy in Buildings and Communities Programme (IEA ECB) [5] has released a publication that surveyed 26 existing buildings from 14 European and Asian countries. Plenty of ventilative technologies such as wind-driven, buoyancy-driven, single-sided, cross, stack, and night ventilation using natural or mechanical forces were used or combined in these exemplary buildings in order to reduce cooling demand and the risk of overheating.

Twelve out of the 26 buildings were selected and summarized in Table 2-4 based on their uniqueness, typicality and representative qualities. The buildings are located in many different climatic areas, from zones with hot summers and cold winters to more temperate zones. The sizes and functions of the selected buildings also span a diverse range, from a single-story kindergarten with an area of only 190 m^2 to a six-story university library with an area of 22,667 m^2. As the results of using various ventilative strategies, some buildings could reach the expected energy consumption. For example, the energy needs for a school building in Lisbon, Portugal, were assessed as low as 6.6 kWh/m^2 for heating and 25 kWh/m^2 for cooling comparing with the regulation for buildings in Lisbon, of 51.5 kWh/m^2 for heating and 32 kWh/m^2 for cooling [39].

On the contrast, another school building in Helsinki, Finland, consumes 63 kWh/m^2 for lighting, HVAC and equipment, while the average electricity usage in Helsinki schools is 52 kWh/m^2 [40].

By reviewing all these low-energy buildings, the following can be summarized:

1) Studies of ventilation in high-rise buildings are essential and lacking.
2) Hybrid ventilation is practical considering the limitations of natural ventilation.
3) Solar chimneys are quite useful for ventilation and enhancement of daylight.
4) It is highly recommended to incorporate CO_2 concentration sensors into the building control system.
5) Energy consumption might not reach the expectation during building operation due to improper system operation. BMS is recommended.
6) Occupant behavior can affect the performance of ventilation systems, especially in low- and mid-rise buildings. It is thus important to instruct occupants on how to behave to maximize the saving of energy.

Table 2-4. Summary table of exemplary existing buildings [5]

No.	Building info	Net floor area & No. of floors	Ventilative technologies	Main components
1	C-DdI Arfrisol PSA Office building, Tabernas, Spain	1,007.4 m^2, one floor	Night cross-ventilation by solar chimneys; Buoyancy-driven cross-ventilation	Solar chimneys; Height difference (high windows)
2	GRUPO LINCE Headquarters, Office building, Valladolid, Spain	1,000 m^2, one floor	Night ventilation; Cross-ventilation; Mechanical ventilation	Lucernaires (for night ventilation); Air collectors integrated in ventilated façade in summer; Internal ventilation grilles for cross-ventilation
3	Police office Schoten, Office building, Schoten, Belgium	2,514 m^2, two floors	High thermal mass; Natural ventilation (day and night) (buoyancy-driven)	Motorized bottom hung windows to supply and exhaust air; internal grilles; BMS with sensors
4	Mellomhagen, School, Larvik, Norway	3,500 m^2, three floors	Hybrid ventilation system (mainly wind-driven cross-ventilation for natural ventilation)	Smart control motorized windows integrated with air exhaust damper; Exhaust fan
5	Solstad, Kindergarten, Larvik, Norway	788 m^2, two floors	Hybrid ventilation system (combined cross- and stack ventilation for natural ventilation)	Smart control motorized windows; Internal hatches; Energy-efficient fan
6	Home for life Residential building, Lystrup, Denmark	190 m^2, two floors	Natural ventilation (single-sided, cross and stack ventilation); Thermal mass	Operable windows on all facades and roof; External solar shadings; Automatic control
7	CHH-Christophorushaus Multifunctional, Miva, Austria	1,215 m^2, three floors + a basement	Mechanical ventilation; Night natural ventilation (stack ventilation)	High level of insulation and limited glazing area; Atrium to enhance airflow movement; Mechanical ventilation with heat recovery

8	Edificío solar XXI, Office and laborary, Lisbon, Portugal,	1,500 m^2, two floors + a basement	Natural ventilation (cross- and stack ventilation); PV panel-assisted ventilation (convection from heat loss); Fan-driven ventilation (through buried pipes)	Openings in roof, facades and between interior spaces; Gap behind PV panels; Fans and buried pipes for air pre-cooling; 5cm EPS external insulation in walls and roof slab
9	Frederick Lanchester Library, Library, Coventry, UK	9,103 m^2, four floors + a basement	Natural ventilation (stack ventilation); Night ventilation	Ventilation towers; Controllable dampers and windows; Tapering light wells for both lighting and ventilation
10	Poikkilaakso School, School, Helsinki, Finland	3,132 m^2, two floors	Mechanical ventilation with heat recovery;	Rooftop air-handling unit; Speed-controlled fan; Management system with sensors
11	Energy Flex House Residential, Taastrup, Denmark	216 m^2, two floors	Two different systems to be compared: Demand-controlled mechanical ventilation with heat recovery; Demand-controlled natural ventilation with night cooling and mechanical free night-time cooling with daytime cold recovery	Automatically controlled windows and skylights; External solar shading; Windows with controllable angle of opening; Sensors in all rooms
12	Library of Shandong Jiaotong University, Library, Jinan, China	22,667 m^2, six floors	Natural ventilation (stack ventilation);	Draft chimney; Controllable shutter grille in atrium air curtain wall; Wind tunnel

2.6 Overview of the EV building and related studies

Concordia University's EV building, one of the latest landmarks of downtown Montreal, was designed and constructed to use natural ventilation in order to reduce cooling load. This 17-story high-rise institutional building houses research labs, studios and offices for faculty and students. The total floor area is approximately 53000 m^2 and the building has two large main façades facing southwest and southeast respectively to maximize solar heat gains in winter. Nevertheless, manually and automatically operated blinds are installed in perimeter zones to prevent overheating and glare in summer. The building has five stacked atriums extending from the second to the sixteenth floor, spanning three floors each and separated with concrete slabs for fire/smoke safety concerns. Each of the five atria has dimensions of 9 m long × 12 m deep × 12 m high, with the glazed façade 35° west of South. To connect all five atria, grilles and motorized dampers can be opened when hybrid ventilation mode is on, causing the whole atrium to serve as a solar chimney. The cooling period for the EV building lasts from April to October or even possibly early November. An estimated 4000-5000 occupants, a huge amount of plug loads plus the high solar gains mean cooling is in high demand for the EV building even while the outdoor air is of a lower temperature than the indoor air. In late 2015, a set of six variable speed fans were installed on the roof of the EV building to enhance air movement and control the ventilation system's performance by integrating the fans into the existing automated system for toggling the atrium grilles and motorized dampers.

Tzempelikos et al. [41] used this building as a simulation case study of preliminary façade and envelope design options during the early design stage. Specifically, the choices of façade, glazing, shading devices and controls, electrical lighting control options and natural and hybrid ventilation were studied and analyzed. The aim was to maximize the use of daylight, eliminate the need for

perimeter heating and reduce peak heating, overall heating and cooling demand. For hybrid ventilation, it was suggested that variable speed fan-assists are necessary to ensure a total flow of 30,000 L/s, while small vents in perimeter offices and inlet grilles with motorized dampers at the ends of the corridors are needed to complement the atrium grilles in order to improve ventilation performance.

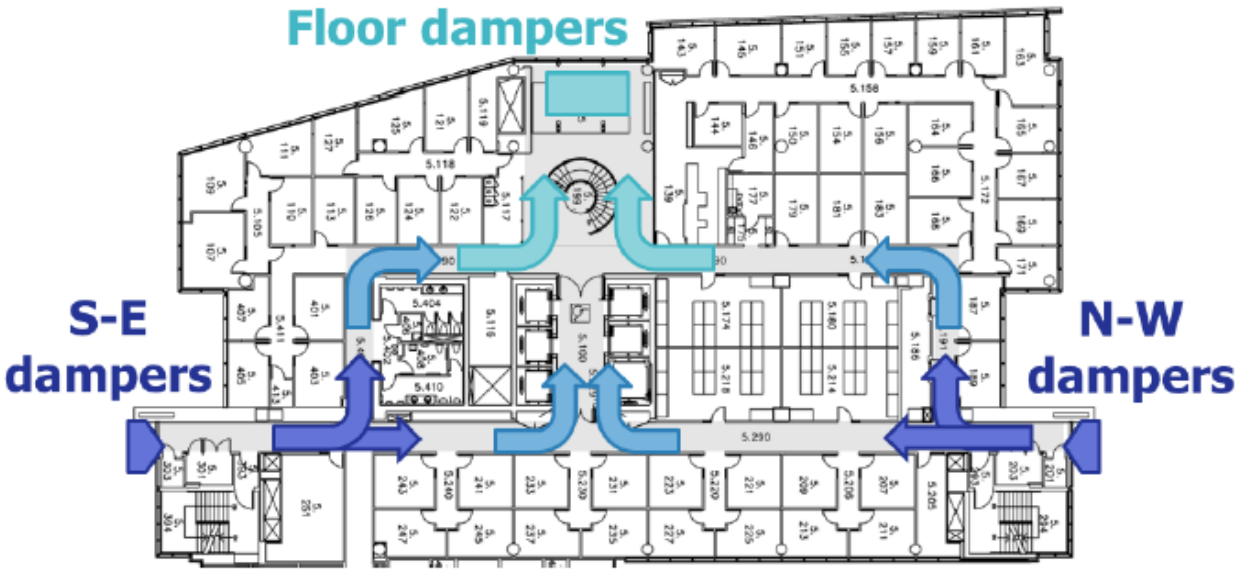

Figure 2-8. Typical floor plan in EV building and expected airflow path [8]

Another study carried out by Mouriki et al. [42] focused on the relation between an atrium with high solar gains and the hybrid ventilation system. By monitoring the performance of the hybrid ventilation system of the EV building, it was learned that there is significant natural ventilation potential in Montreal from April to October. In particular, during the months of June, August and September, the natural ventilation mode was ON 45-51% of the time when the outdoor temperature was between 15°C and 25°C and the relative humidity was less than 60%. It was found that the air temperature stratification difference in an atrium could be 2°C whether the natural ventilation

system was ON or OFF. In addition, a very large night cooling potential was observed with night air temperatures reaching as low as 12°C during the cooling season. This can be used to further cool the building mass from midnight to morning.

A further study based on the previously mentioned research showed that the in-flowing air stream has a much higher cooling capacity at lower temperatures, resulting in higher amounts of cooling stored in the thermal mass. More precisely, an air stream at 12°C could surprisingly remove 5 times more heat than an air stream at 18°C. Karava et al. [43] concluded that their findings are worth using to generalize some guidelines for commercial buildings with similar hybrid ventilation systems since it has been proven that free cooling can cover a significant part of the cooling requirements.

In this study, the overall concept of the EV building's hybrid ventilation system was also well-summarized. When the outdoor temperature was between 15°C to 25°C and the RH was less than 70%, the system would:

(a) open the atrium grilles and motorized dampers at two ends of the corridors;
(b) decrease the mechanical airflow rate of the air supply outlets in the atrium to the minimum number;
(c) open the exhaust vents on the top atria open;
(d) stop the air supply to the corridors.

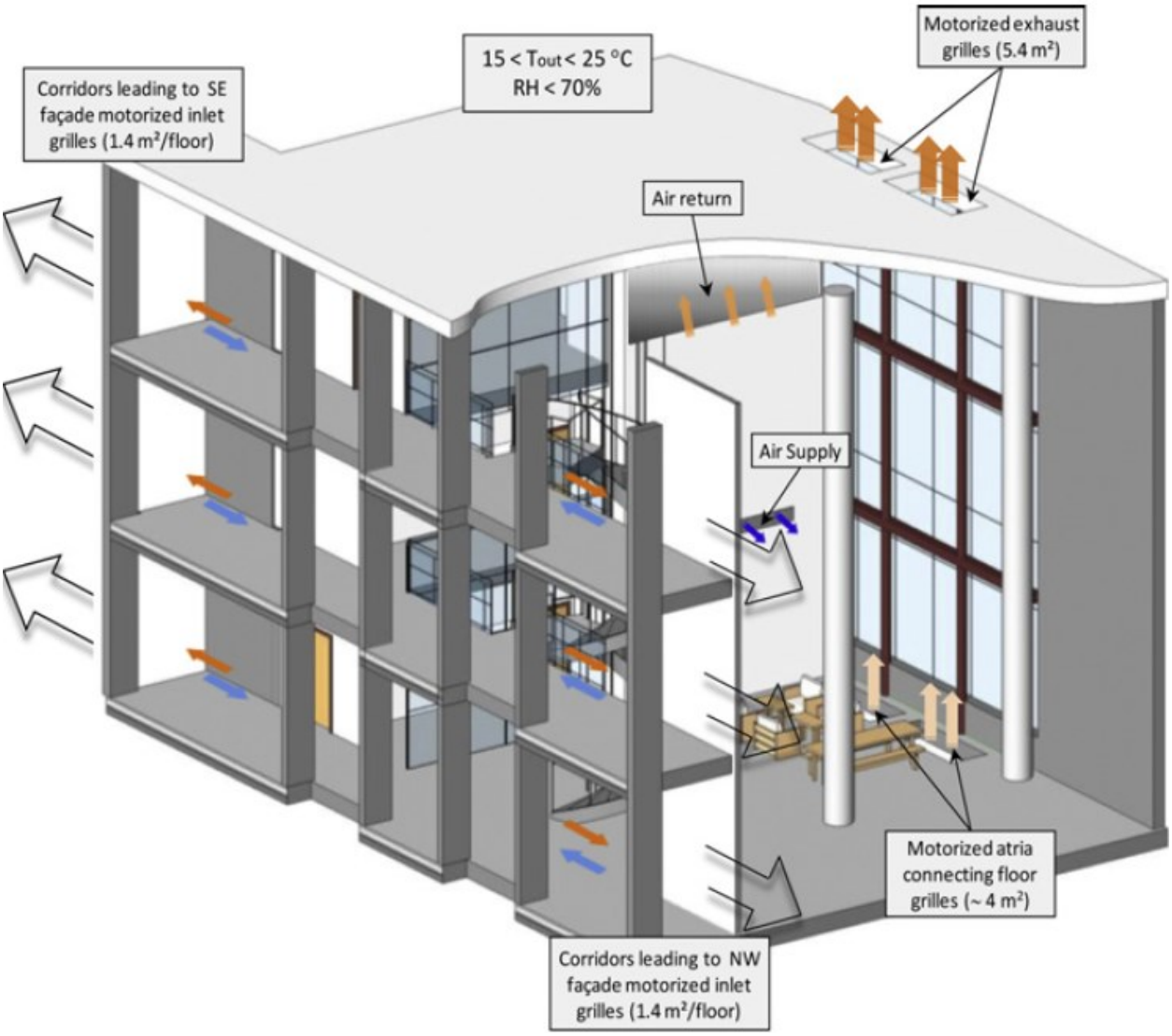

Figure 2-8. Hybrid ventilation system concept of EV building [43]

2.7 Conclusion

In general, outdoor weather conditions such as outdoor air temperature, wind velocity and wind direction are essential for utilizing natural ventilation potential. The types of openings (mainly windows) specific to each building can decide the exact airflow rate coming through. Thermal

comfort is the most significant factor in determining whether the ventilation performance in a building is acceptable to the occupants.

By reviewing all the existing airflow flow rate equations for natural ventilation, it shows the ubiquity of limitations among the empirical expressions. For instance, in some of the general empirical models, the effects of the wind incidence angle (wind direction) which might make substantial discrepancy as to the ventilation airflow rate. Overall, there is a lack of an evaluation method in the form of empirical equations to determine natural ventilation potential. Functionally, the method should cover coefficients selection to energy saving potential calculation. In addition, considering it would be mainly applied in the early design stage, this evaluation method needs to be quick and accurate comparing to the equations with very few variables and/or coefficients.

Through studying on the exemplary existing buildings, it indicates the viability and great potential of utilizing natural and/or hybrid ventilation system in terms of saving energy. Specifically, solar chimney plus mechanical exhaust fan is proved to be a practical application in the buildings using hybrid ventilation system. The concept of the EV building hybrid ventilation system was illustrated through previous studies. As a high-rise institutional building, the EV building could be an ideal case study and supplement to IEA-ECB's study since a hybrid ventilation system with solar chimney is using in EV building. In order to optimize the performance of hybrid ventilation system and maximize energy saving in EV building, it requires a comprehensive model with better accuracy calibrated by experimental data.

3 Natural Ventilation Study in Early Design Stage

3.1 Problem statements

Since the use of natural (or hybrid) ventilation is closely related to the wind regime and the building's location, orientation, shape, window/wall ratio etc., a decision regarding its use needs to be made during the early stages of building design, i.e. the conceptual design stage. Therefore, the analysis of the energy-saving potential of natural ventilation demands a quick and relatively accurate method, such as a set of empirical equations, to determine natural ventilation airflow rates and compare ventilation strategies.

A review of previous studies [15], [20], [21], [28]–[33], [36], [37], shows that plenty of empirical equations exist for both single-sided ventilation and cross-ventilation, which are mainly driven by wind, buoyancy or a mix of the two. However, each of the empirical equations has its own limitations. In other words, there is no general equation which can be directly used with a clear guideline for the selection of coefficients. The foundation of this study is to determine a guideline for coefficient selection based on existing equations for naturally ventilated buildings with a common shape. Eventually, based on empirical equations with newly developed coefficients, a quick method with acceptable accuracy was developed to estimate the natural ventilation energy saving potential.

3.2 Methodology of evaluation approach

For the purpose of generalization, only wind-driven natural ventilation is considered in this study, as the effective use of the force of buoyancy depends more greatly on the building's interior layout.

The building is assumed to be flat, symmetrical and non-high-rise, and the effect of internal partitions is neglected. The two equations listed below were selected from the literature [32], [34] because of their better applicability comparing to others, for the separate calculation of wind-driven single-sided ventilation and cross-ventilation flow rates:

Single-sided ventilation:

$$Q = \frac{dv}{dt} = \pm C_D * A * \sqrt{\left| U^2 - \left(\frac{2 * \gamma * P_a}{\rho * V} \right) * \nu \right|}$$

Eq. 3-1

$$\overline{Q_{eff}} = \frac{1}{2} * f * Q$$

Eq. 3-2

Cross-ventilation:

$$Q = \sqrt{\frac{Cp_1 - Cp_2}{\frac{1}{A_1^2 * C_{D_1}^2} + \frac{1}{A_2^2 * C_{D_2}^2}}} * U_r = \sqrt{\frac{\Delta C_p}{\frac{1}{A_1^2 * C_{D_1}^2} + \frac{1}{A_2^2 * C_{D_2}^2}}} * U_r$$

Eq. 3-3

Specifically, f and ΔC_p were selected for two ventilation strategies since they are the two key undetermined coefficients for calculating the air flow rates. Although many researchers were interested in researching these two coefficients and carried out some wind tunnel experiments based on cubic shape models due to the dimensional limits[32], [44]–[46], there are as of yet no universal standards for determining them. It is commonly believed that they are highly dependent on the building configuration, location of openings, opening configuration, etc.

To summarize the whole process of evaluating natural ventilation potential, see the flow chart below:

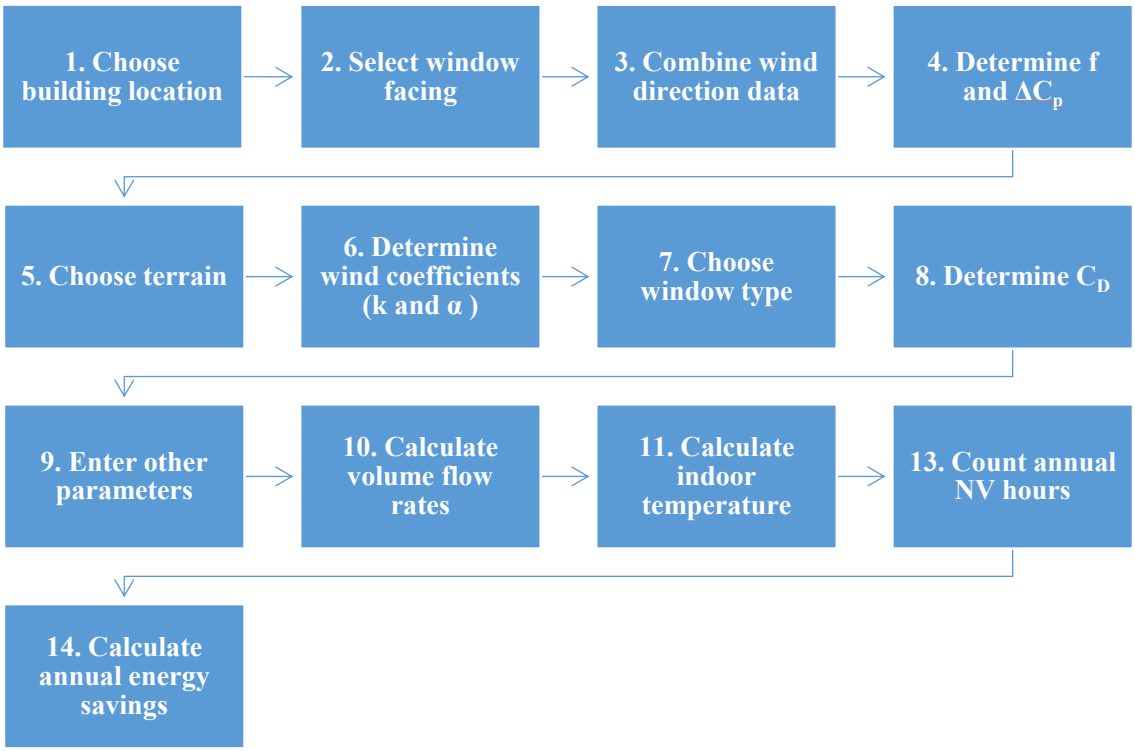

Figure 3-1. Schematic approach to evaluating natural ventilation potential

Other critical coefficients such wind velocity coefficients $K$and α for wind profile correction and discharge coefficients C_D for window type selection are determined according to literature [15], [19], [47] as introduced in previous chapter.

Once the air flow rates through the openings are simulated, two key coefficients f and ΔC_p for ventilation can be calculated accordingly. By applying cubic spline interpolation, coefficients f and ΔC_p along all incidence angles (0° - 180°) can then be generated.

Nonetheless, the internal heat gain Q_{in} is considered when determining the viability of natural ventilation, which is quantified as annual available natural ventilation hours. Specifically, indoor

air temperature is used to determine whether natural ventilation is acceptable for the occupants of the building.

$$Q_{in} = m \times C \times \Delta T = m \times C \times (Ti - To)$$

Eq. 3-4

$$Ti = \frac{Q_{in}}{m \times C} + To$$

Eq. 3-5

For simplicity, some parameters and coefficients are assumed to be constant in the calculations, while the others such as wind velocity, wind direction and outdoor temperature are based on 10 years hourly meteorological data [13].

Table 3-1. Constants assumed in calculation

Parameter	**Number**
outdoor air pressure (kPa)	101.3
specific heat (kJ/kg·K)	1.005
molecular weight of air (kg/kmol)	29
ideal gas constant (J/kmol·K)	8314.5

Once all the calculations are completed based on hourly natural ventilation rates, the indoor air temperature can be determined for each hour. Therefore, the annual available natural ventilation hours would be counted according to the building occupants' acceptable indoor temperature range.

For simplification, natural ventilation potential only counts when the indoor air temperature is within a certain acceptable range based on 10 years of hourly historical weather data.

3.3 Wind tunnel tests and validations

To develop the evaluation approach, the use of computational fluid dynamics (CFD) is necessary and crucial since the utilization of CFD has been widely used as an effective method [48]–[55] for the simulation of natural ventilation. In this study, ANSYS FLUENT 16.2 was used for all simulations. There are two main turbulence models, Reynolds-averaged Navier-Stokes (RANS) and Large Eddy Simulation (LES), to choose between for the simulation [54]–[60]. Thus, in order to determine which model is more efficient to achieve the final objective, two cases were conducted for validation using both turbulence models.

3.3.1 Single box model

Two 250 mm × 250 mm boxes were created. One has only one 84 mm × 125 mm opening in one wall, and the other has two openings of the same size in opposite walls. The thickness of the walls was neglected since heat transfer is not considered in this case.

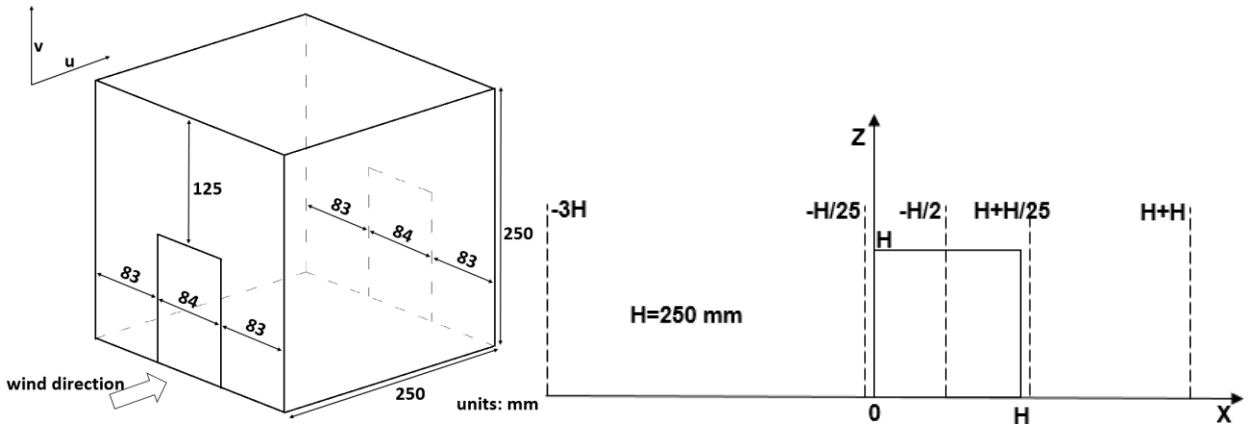

Figure 3-2. Schematic view of single-opening model and air velocity measurement locations

In the CFD simulation, the building model was placed within a larger computational domain which had an upstream length of 4H (H=250 mm), a downstream length of 8H, a lateral length of 4H on both sides of the building, and a vertical length of 3H above the building height. The velocity in the X axis, U, was measured at five locations which were all at the center plane of the model along the streamline (Y axis).

After acquiring the simulation results, the mean velocity distributions were compared with the wind tunnel test results from [52]. Both LES and RANS (two-equation standard $k-\varepsilon$ models, precisely) were used and the comparisons are demonstrated below (Figure 3-3):

As can be seen from the figures below, the distributions behind the building model were overestimated, especially in LES model results. This was potentially caused by the difference between the wind profile (resulting from linear-regression of experimental data) applied in the simulation and in the real experimental setting. The overall arrangement between the CFD predictions (LES and RANS) and experimental results is fairly similar along the streamline direction, which is close to the results from [52]. The difference in results is not obvious between two models.

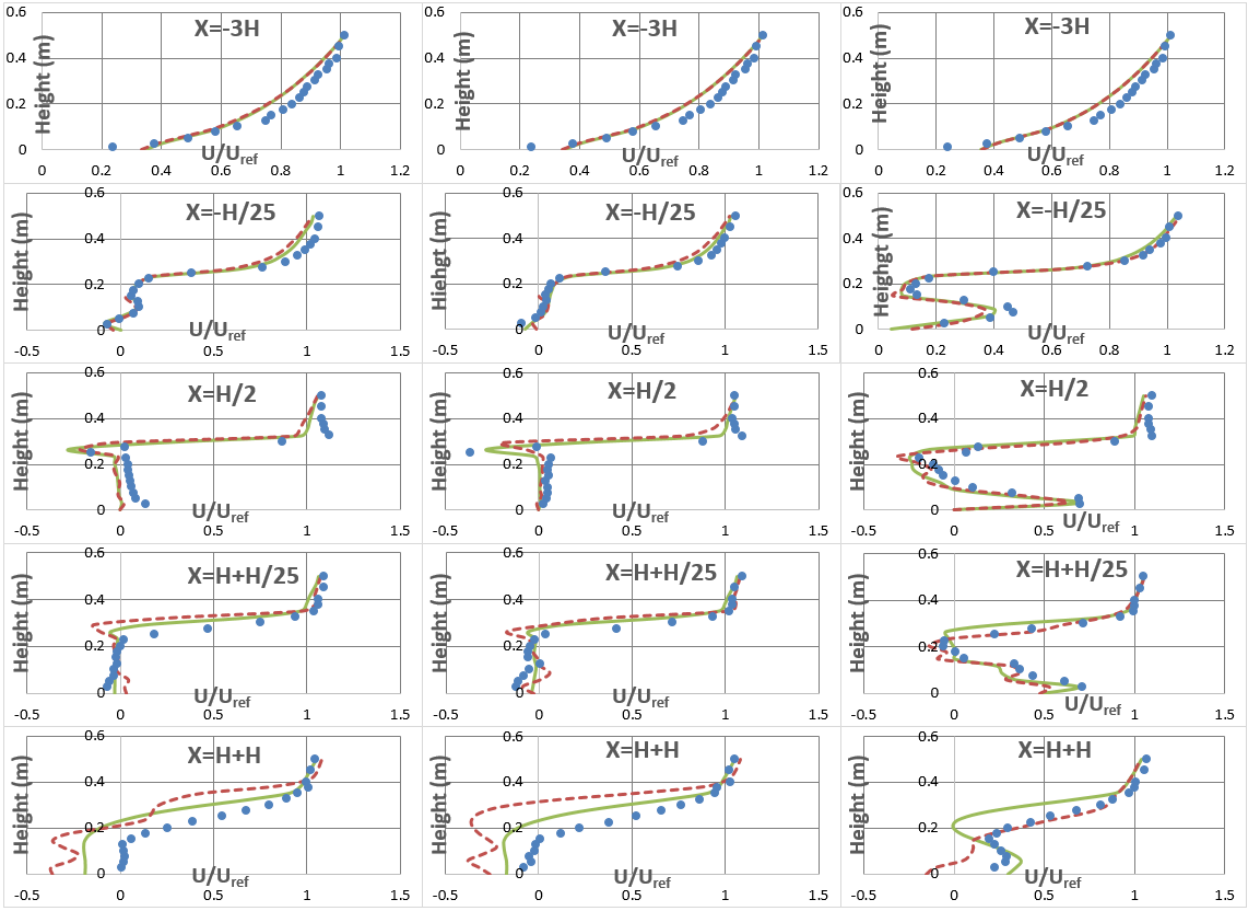

Figure 3-3. Mean velocity distributions for windward, single-sided ventilation (left column); leeward, single-sided ventilation (middle column) and cross-ventilation (right column). Dots: Experiment; Solid line: RANS model; Dashed line: LES model.

3.3.2 Block model with surroundings

In order to improve the accuracy of this study, a series of wind tunnel experiments were carried out using a commercial wind tunnel in an engineering consulting firm [61]. The dimensions of the wind tunnel were 8 ft x 6 ft x 100 ft (W x H x L) with a 40 ft upwind portion.

The core building model (as the red block shows at the bottom of Figure 3) used in the wind tunnel experiments was 266.7 mm x 83.3 mm x 48 mm (L x W x H) with a scale of 1:300. The exponent (α) is set to be 0.25 for the wind profile in both experiments and simulations. 111 pressure sensors,

each tested for all wind directions (36 directions at 10° increments) were placed on the test model. The wind tunnel experiment results are finalized with the pressure coefficient C_p values and normalized with the wind speed at reference height.

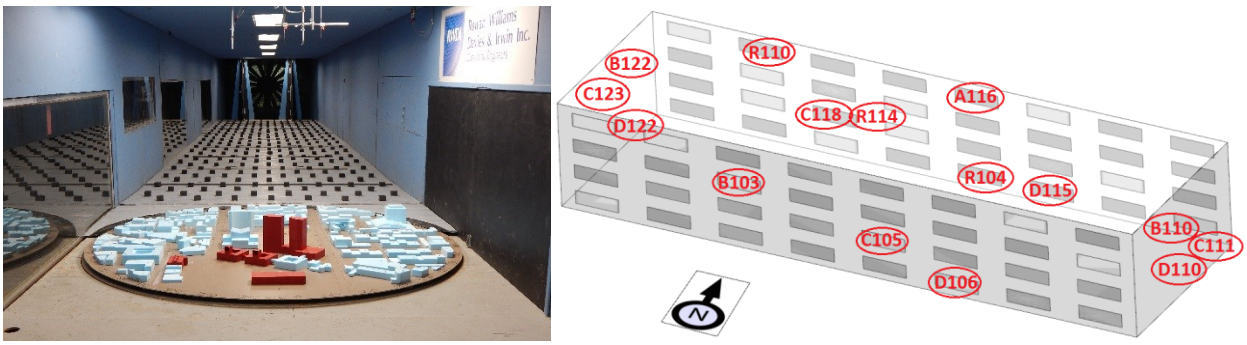

Figure 3-4. Wind tunnel model view from south and location of selected sensors [61]

After the wind tunnel experiment results were provided, CFD simulations with the same conditions as the experiments were performed for validation. In the simulations, a transient state model with large eddy simulation (LES) was selected for relatively accurate natural ventilation simulation considering the complexity of the surrounding models. The full model used in the simulations contains approximately 750,000 elements and more than 12,000 time steps with each time step at 0.1 seconds. The final results are the average number of the last half of the time steps.

A suburban wind profile was chosen for the wind tunnel experiments. Thus, according to the information provided, the wind profile power law used in the computer simulations was:

$$U = 15 \times (\frac{Z}{600})^{0.25}$$

Eq. 3-4

However, in the wind tunnel test results, the pressure coefficient C_p values were scaled to the wind speed in an airport (open wind profile with $\alpha = 0.14$) at the height of 10 meters. Therefore, the reference wind speed equals:

$$U_{airport} = 15 \times (\frac{10}{600})^{0.14} = 8.46\ m/s$$

To normalize the C_p values, an equation was applied as below, where the static pressure Ps could be read from the CFD simulation results.

$$C_p = \frac{P_s}{0.5 \times \rho \times U_{airport}^2}$$

Eq. 3-5

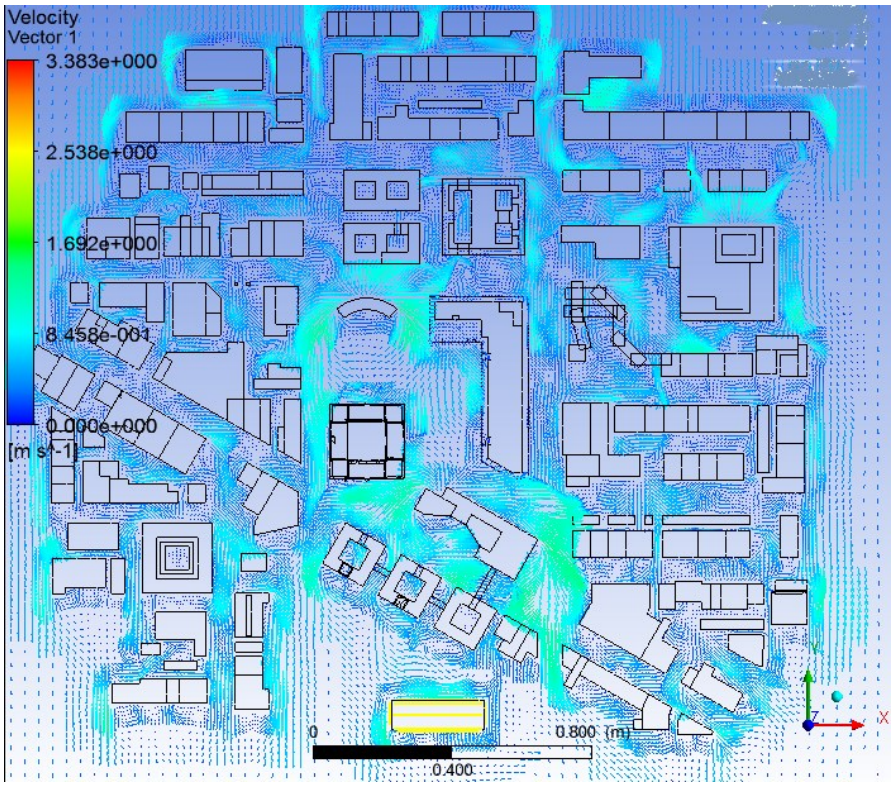

Figure 3-5. Flow pattern of CFD simulation in XY plane

Figure 3-6 compares the C_p results between the simulations and the experiments. For conciseness, 15 well-distributed sensors were selected and illustrated where the solid blue line and red dots demonstrate the simulation and experiment results respectively from 0° to 350°.

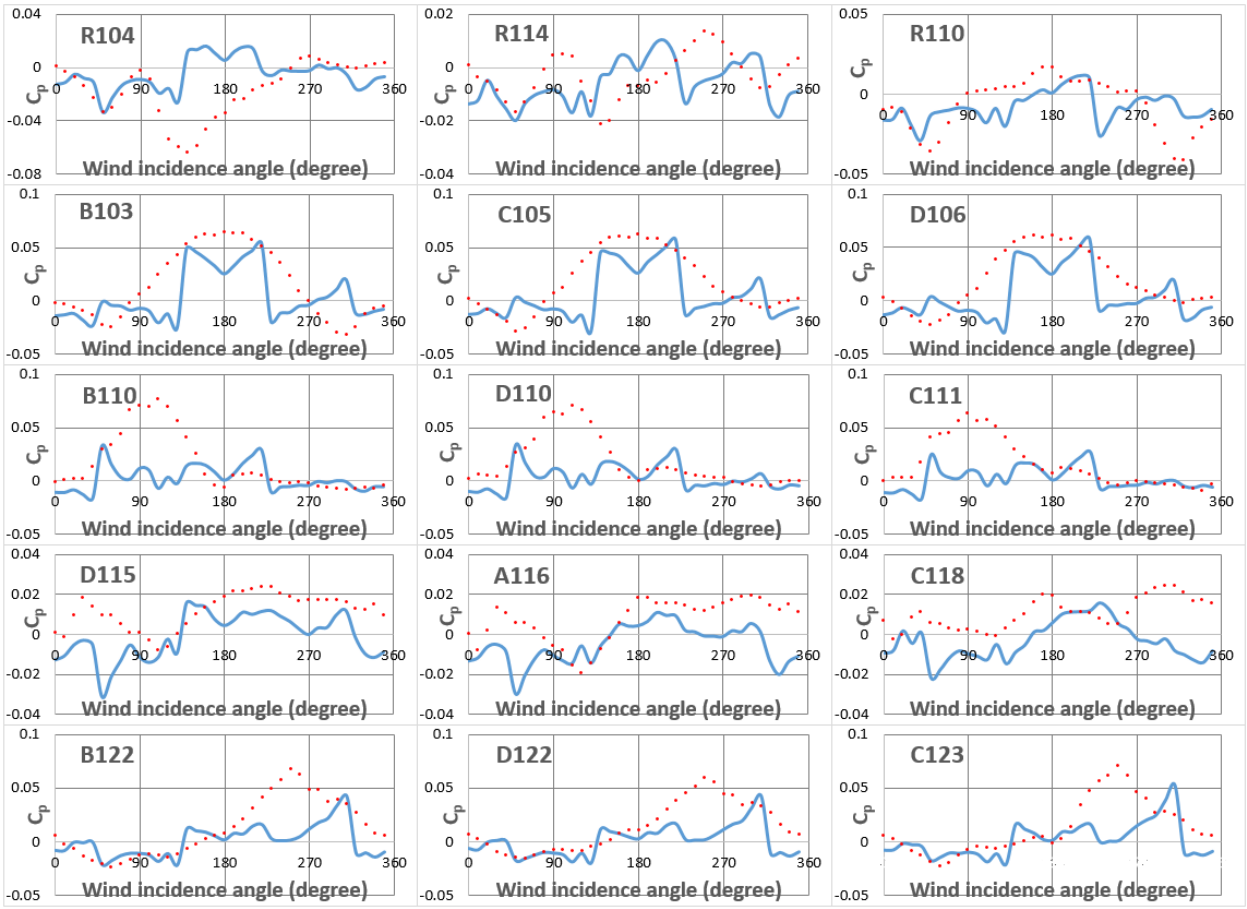

Figure 3-6. C_p values on the roof and south, east, north and west facade (from the first row to the fifth row respectively) of the test model. Dots: Experiment; Solid line: CFD simulation (LES model).

As can be found from the figure above, the comparison shows a rough agreement between experimental data and simulation result. However, disparities do exist in many locations. This is mainly due to the limited mesh quality of the surrounding models which may influence the airflow

surrounds the core building model. Since most of these models are larger, higher and more complex than the core model, it requires huge amount of meshes and much longer time for them to be simulated more accurately. Otherwise, the error accumulates remarkably and the simulation accuracy would be affected significantly. Besides, there was another disparity between the sensor locations in the experiments and the sampling locations in the simulations due to the limitations of the software. In experiments, all sensors were mounted to the surfaces of model. However, in computational simulation, the distance between sampling location and model surface cannot be less than 10^{-2} m which is not negligible in such small scale experiment. Additionally, whether there was any experimental error is uncertain.

Overall, by analyzing the validation results, considering the final building model has no surroundings. Thus, the RANS standard $k-\varepsilon$ model was selected to conduct the rest of simulations considering it is acceptably accurate, time-efficient comparing to the LES model [62], [63].

3.4 Simulation and Results

In this study, ANSYS Fluent 16.2 was used to simulate and determine airflow rates through building openings to obtain the two key coefficients f and ΔC_p. As mentioned previously, the effects of buoyancy flow and internal building layout are neglected.

3.4.1 Geometry and meshing

The standard building is 80 m x 25 m x 14.4 m (L x W x H) and is placed within a larger computational domain which has an upstream length of 4W, a downstream length of 6W, a lateral

length of 4L on both sides and a vertical length of 4H above the building height. The building has four floors and thirty-two windows (6 m x 1.8 m) on each long side. Thus, there are sixty-four windows in total. With consideration to the balance between energy-saving and daylighting requirements, the window-to-wall ratio (WWR) is set to be 30% in all scenarios [64]–[66].

Considering the model is a cube, CutCell was selected as the assembly meshing method. Most of the meshes are hexahedral, while a few of them are unstructured. In total, approximately 500,000 meshes were generated with a minimum size of 0.3 m.

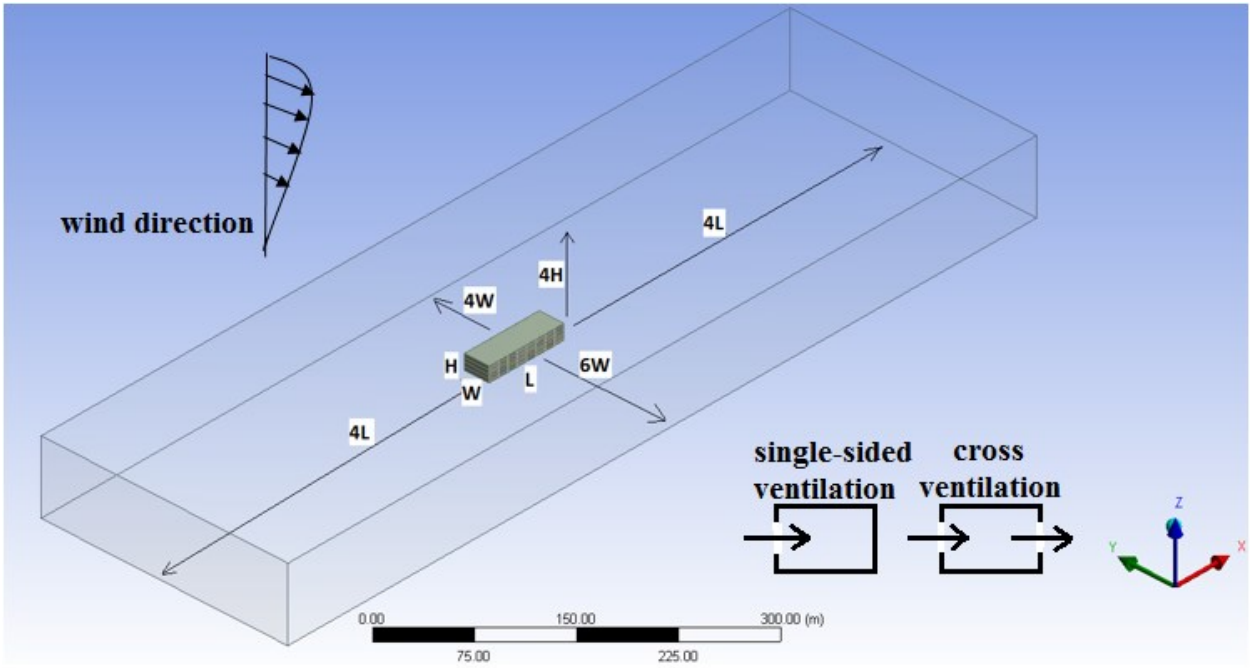

Figure 3-7. Schematic view of the model with outer domain (W=width, L=length and H=height)

3.4.2 Turbulence model

Due to a synthesis of different factors such as feasibility and computation time, a steady state Reynolds-Averaged Navier-Stokes (RANS) standard $k-\varepsilon$ turbulence model was selected. The

governing equations for the incompressible turbulent flow encountered in this research are expressed as follows:

Continuity equation:

$$\frac{\partial}{\partial x_i}(\overline{\rho u_i}) = 0$$

Eq. 3-6

Momentum equation:

$$\frac{\partial}{\partial x_j}(\overline{\rho u_i u_j}) = -\frac{\partial \overline{p}}{\partial x_i} + \frac{\partial}{\partial x_j}\left[\mu\left(\frac{\partial \overline{u_i}}{\partial x_j} + \frac{\partial \overline{u_j}}{\partial x_i} - \frac{2}{3}\delta_{ij}\frac{\partial \overline{u_l}}{\partial x_l}\right)\right] + \frac{\partial}{\partial x_j}\left(-\overline{\rho u'_i u'_j}\right)$$

Eq. 3-7

Since the energy equation is redundant in the case of incompressible fluid flow, $-\overline{\rho u'_i u'_j}$ is the Reynolds stresses. By utilizing the Boussinesq assumption, the Reynolds stresses can be given by:

$$-\overline{\rho u'_i u'_j} = \mu_t\left(\frac{\partial \overline{u_i}}{\partial x_j} + \frac{\partial \overline{u_j}}{\partial x_i}\right) - \frac{2}{3}\left(\rho k + \mu_t \frac{\partial \overline{u_i}}{\partial x_i}\right)\delta_{ij}$$

Eq. 3-8

It can be found that determining μ_t is the key to determining the turbulence. Therefore, in the standard k-ε turbulence model, the turbulent kinetic energy (k) and its rate of dissipation (ε) are obtained from the transport equations below [67]:

$$\frac{\partial}{\partial t}(\rho k) + \frac{\partial}{\partial x_i}(\rho k u_i) = \frac{\partial}{\partial x_j}\left[\left(\mu + \frac{\mu_t}{\sigma_k}\right)\frac{\partial k}{\partial x_j}\right] + G_k + G_b - \rho\varepsilon - Y_M + S_k$$

Eq. 3-9

$$\frac{\partial}{\partial t}(\rho \varepsilon) + \frac{\partial}{\partial x_i}(\rho \varepsilon u_i) = \frac{\partial}{\partial x_j}\left[\left(\mu + \frac{\mu_t}{\sigma_\varepsilon}\right)\frac{\partial \varepsilon}{\partial x_j}\right] + C_{1\varepsilon}\frac{\varepsilon}{k}(G_k + C_{3\varepsilon}G_b) - C_{2\varepsilon}\rho\frac{\varepsilon^2}{k} + S_\varepsilon$$

Eq. 3-10

Therefore, the turbulent viscosity (μ_t) could be computed by combining k and ε as follows:

$$\mu_t = \rho C_\mu \frac{k^2}{\varepsilon}$$

Eq. 3-11

where $C_{1\varepsilon} = 1.44, C_{2\varepsilon} = 1.92,\ C_\mu = 0.09, \sigma_k = 1.0$ and $\sigma_\varepsilon = 1.3$ are default constants.

The standard wall functions were employed for near-wall calculation.

3.4.3 Boundary conditions and discretization scheme

The airflow model was solved using the conditions for the velocity inlet, pressure outlet and solid walls. For the velocity inlet, a user-defined function of the wind profile for an open area was employed where the exponent is 1/7 and the wind velocity at reference height equals 3.8 m/s (derived from meteorological data).

The common SIMPLE pressure-velocity coupling algorithm was used to solve the airflow equations. All residuals reached at least 5×10^{-4} of convergence. Table 3-4 demonstrates the discretization scheme applied in the simulations.

Table 3-2. Discretization scheme

Pressure	Momentum	$\boldsymbol{k}$	$\boldsymbol{\varepsilon}$
Standard	2nd-order upwind	1st-order upwind	1st-order upwind

3.4.4 Results

Firstly, in order to investigate the meshing independency, two angles of 45° and 90° with almost three times the number of meshes used in the original model were applied to compare the airflow rates for both single-sided and cross-ventilation as shown in Figure 6 below:

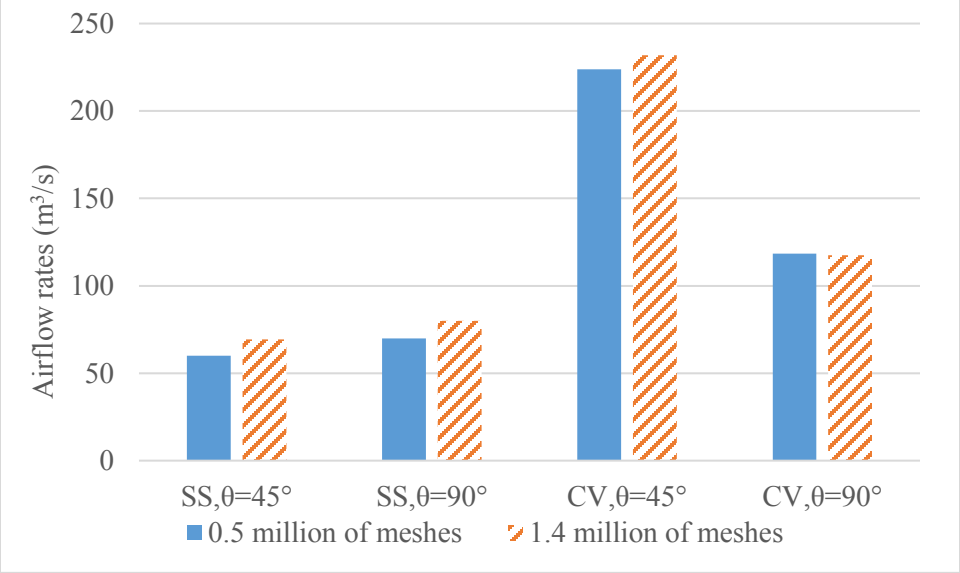

Figure 3-8. Comparison of airflow rates with different numbers of meshes. SS: Single-sided ventilation; CV: Cross-ventilation

Figure 3-7 above shows that the difference varies from 0.07% to 15% which is acceptable considering the difference in time consumption between the two scenarios.

Figure 3-9 illustrates the simulation results of airflow rates for single-sided and cross-ventilation with different numbers of building floors at every 15 degrees of wind incidence angle. Then, by utilizing Equation 3-1, 3-2 and 3-3, coefficient f and coefficient ΔC_p (see Figure 3-10) could be determined with the use of few number constants (i.e. Outdoor air pressure P_a=101.3 kPa, specific heat C=1.005J/(kg·°C) and the ratio of the specific heat of air γ=1 since the ambient temperature in all simulations is constant).

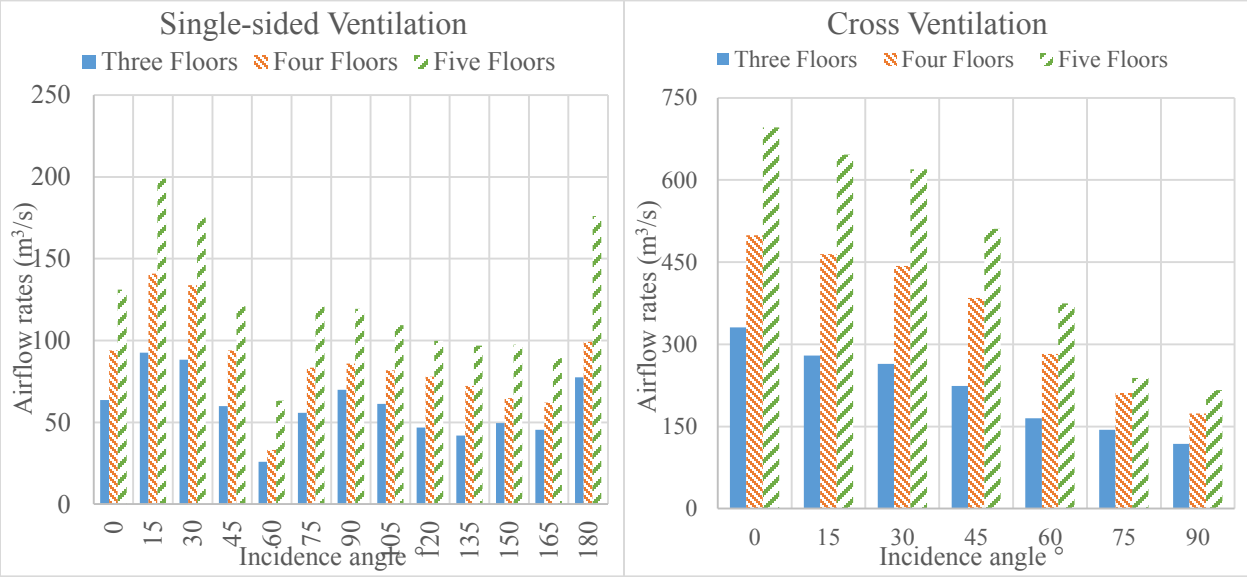

Figure 3-9. Airflow rates for single-sided ventilation (left) and cross-ventilation (right) under different scenarios

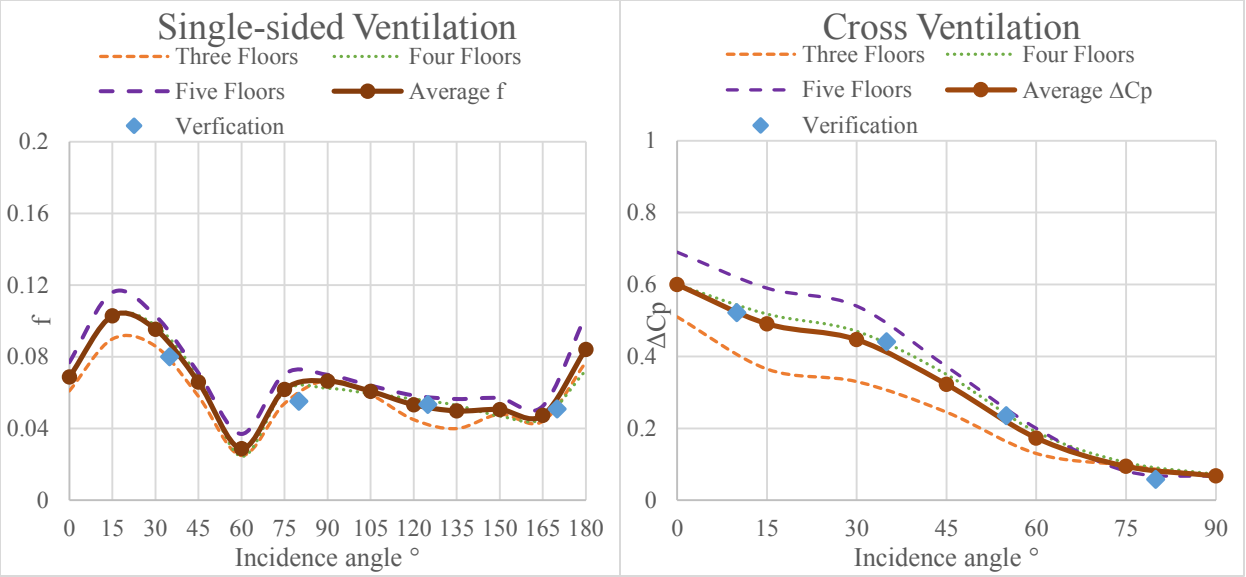

Figure 3-10. Coefficients f for single-sided ventilation (left) and ΔCp for cross-ventilation (right) under different scenarios

To verify the continuity of coefficient ΔC_p and coefficient f, four different angles were selected to be simulated and compared with the existing results as shown in Figure 3-10. As can be seen, the distribution of verification results basically corresponds with the existing arrangement. In addition, the values of ΔC_p and f are axisymmetrical based on the incidence angle of 90° and 180° respectively because the building and its windows are assumed to be symmetrical by default.

3.5 Case study and Discussion

As an application of this study, a fast evaluation tool was developed in the form of empirical equations based in Microsoft Excel for the quick estimation of annual natural ventilation and energy saving potential. A simplified four-story rectangular building located in an open area in Toronto was chosen as a base case for the tool.

Table 3-3 below defines the baseline input parameters such as the size of the building, window-to-wall ratio and the type of window.

Table 3-3. Baseline input parameters

Building location:	Toronto	**Window-wall ratio:**	40%
Terrain:	Open area	**Internal heat gain (W/m^2):**	70
Window type:	Casement	**Min. design temp. (°C):**	21.5
Building size (m):	80×25×14.4	**Max. design temp. (°C):**	27.8
Number of floors:	4	**Number of rooms per floor**	30
A/C consumptions per room (kW):	1.06		

After inputting key building parameters, the corresponding coefficients (i.e. ΔC_p, f and C_D etc.) from the tables and figures above were then applied. Equation 3-1, 3-2 and 3-3 were then used to calculate hourly airflow rates for both single-sided and cross-ventilation since the input parameters were known from Table 3-3. Equation 3-6 was then applied to calculate hourly indoor temperature using 10 years of hourly meteorological data. The annual available natural ventilation hours and energy saving for this building are shown below with different window facing and ventilation strategies.

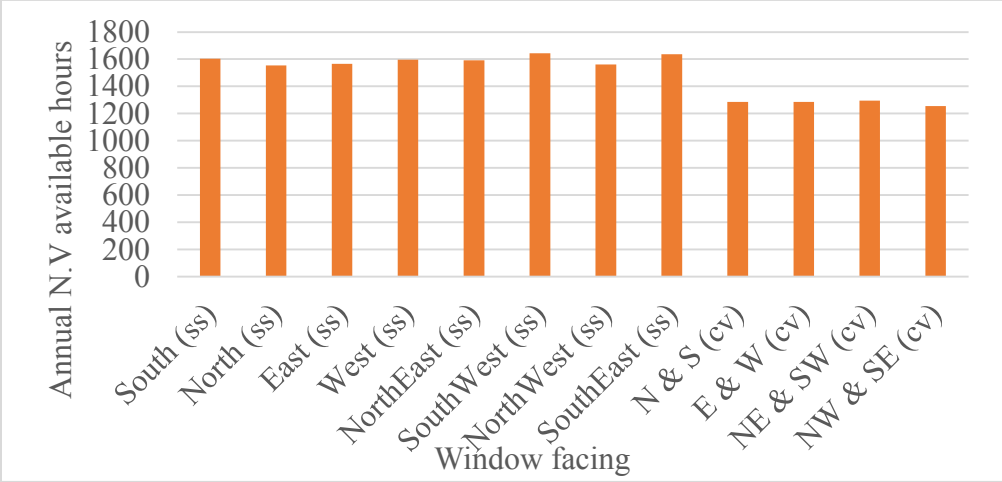

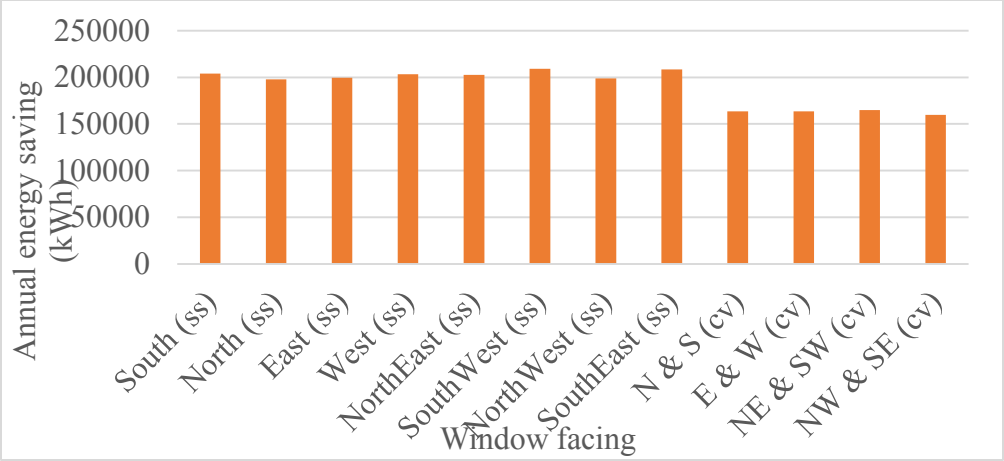

Figure 3-11.Statistics of annual available natural ventilation hours (top) and energy saving (bottom)

As can be seen from Figure 3-11, a building in Toronto with windows facing southeast has a maximum natural ventilation potential of 1644 annual available hours under the single-sided ventilation strategy with the current settings. Specifically, the indoor design temperature range (21.5°C – 27.8°C) achieved 80% thermal comfort acceptability based on the Adaptive Model for naturally ventilated buildings [22], [23], [25], [68]. This building is set to be an office building with a combined internal heat gain of 70 W/m^2 [69] [70], which affects natural ventilation potential significantly and will be discussed later. Additionally, annual energy saving calculations are directly related to A/C unit energy consumption in addition to the total number of rooms and annual available natural ventilation hours. In this case, the A/C unit energy consumption is 1061 watts (EER of 11.3) which represents the most common product on the market for middle size offices.

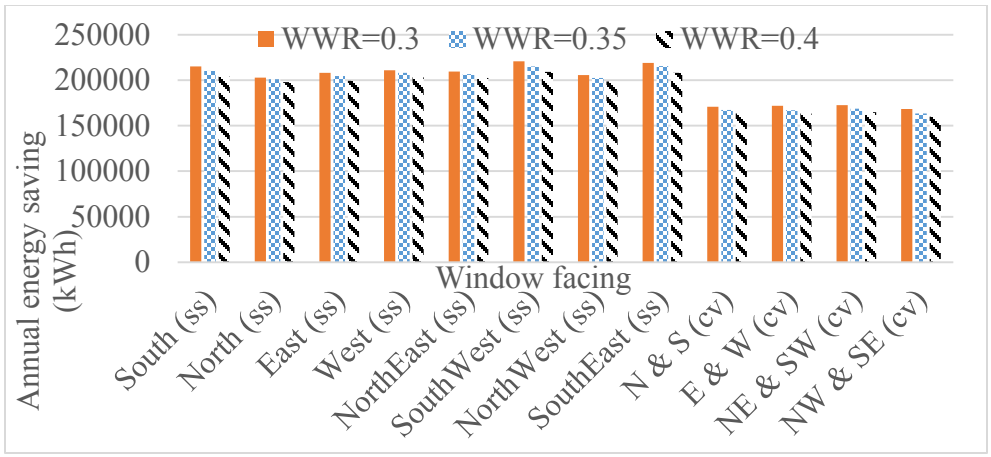

Figure 3-12. Annual available natural ventilation hours under different window-wall ratios

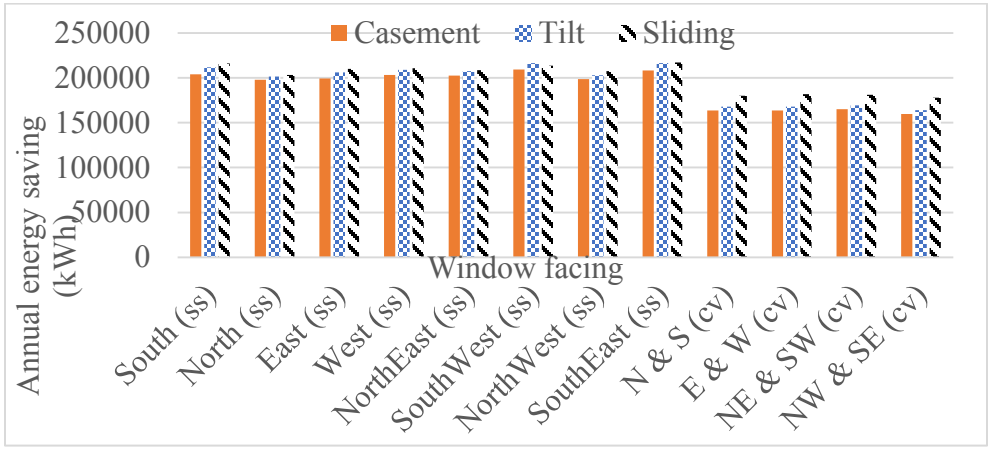

Figure 3-13. Annual available natural ventilation hours under different window types

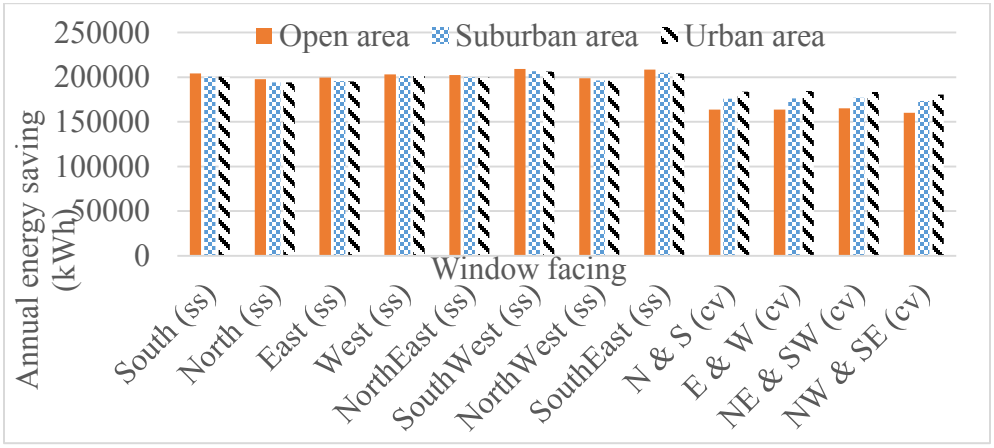

Figure 3-14. Annual available natural ventilation hours with different building terrain

Figure 3-12 to Figure 3-14 show that a smaller window-wall ratio tends to mean a greater amount of energy saved. Nevertheless, an addendum to ASHRAE 189.1, “Standard for the Design of High-Performance, Green Buildings Except Low-Rise Residential Buildings" twice proposed that the window-wall ratio be decreased from 40% to 30% in order to reduce building energy consumption. In other words, an explanation for this tendency could be that lower flow rate leads to more energy saving. By comparison, a WWR of 0.3 has about 5% more energy saving potential than same building but with 0.4 of WWR and this building could save up to 10% of energy by using sliding windows rather than the others. Besides, building terrain only make obvious difference in cross ventilation. To further explain, A WWR of 0.3, sliding windows and an urban environment mean a smaller opening area, a smaller C_D and slower wind velocity which result in lower flow rate. Thus, when the internal heat gain Q_{in} is constant, lower flow rate m causes a higher temperature difference ΔT, as expressed in Eq. 3-5.

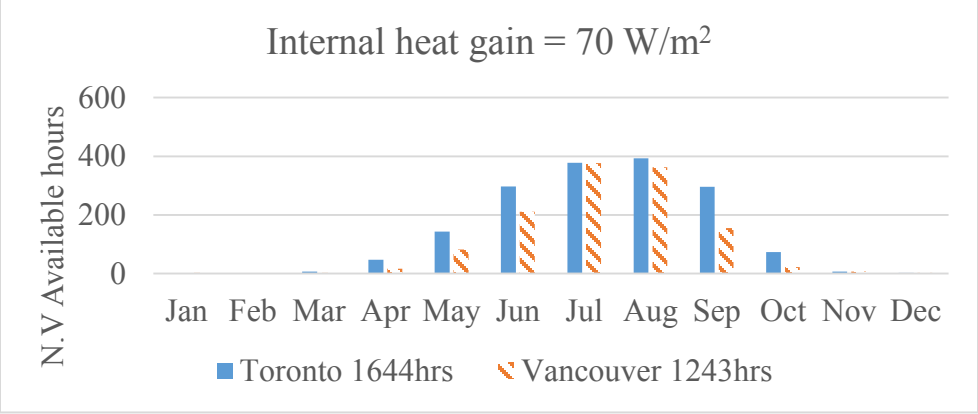

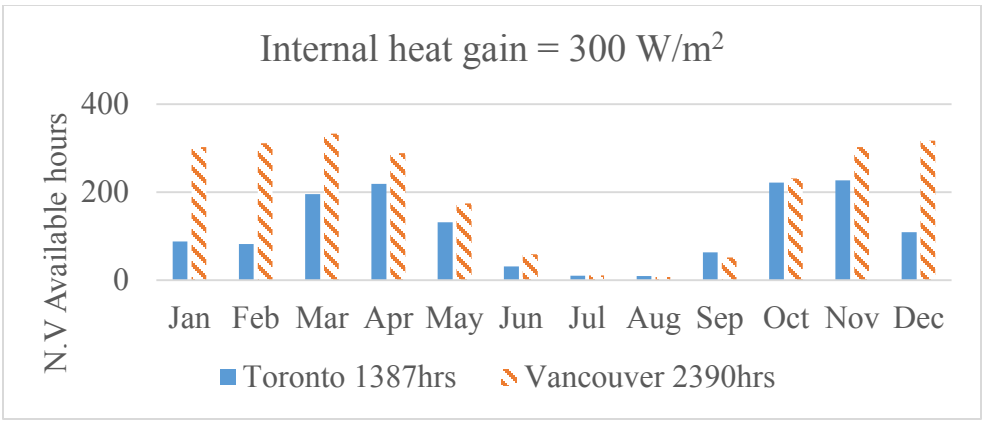

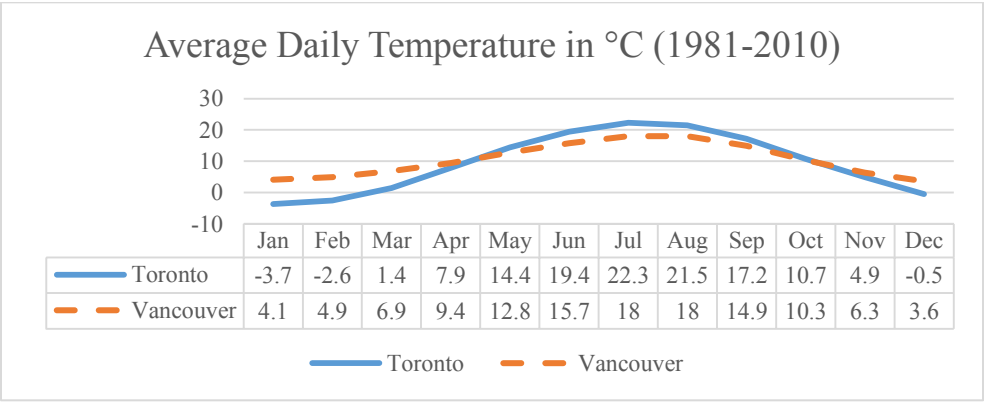

Figure 3-15. Comparison at Q_{in}=70W/m^2 (top), Comparison at Q_{in}=300W/m^2 (middle) and Daily temperature data (bottom)

The scenario with the maximum natural ventilation potential in the base case, which is the scenario of single-sided ventilation with windows facing southeast, was chosen as the baseline. The same parameters were then applied to Vancouver for the sake of comparison. The top figure shows the natural ventilation potential in Vancouver is lower than in Toronto and all the available hours are concentrated in the traditional period for natural ventilation use (summer plus the transition season). This is because the average daily temperature in Vancouver is lower than in Toronto and thus indoor air temperature in Vancouver is also lower than in Toronto with Q_{in} = 70 W/m^2. In other words, Vancouver needs a higher Q_{in} to achieve the same natural ventilation potential as Toronto. However, when Q_{in} is high enough, as in a high-tech office or data center which normally

has a Q_{in} even higher than 300 W/m^2, the natural ventilation potential of Vancouver would be much higher than Toronto's with the potential mainly being distributed in winter and the transition season due to the higher average daily temperature as in the middle figure shown above.

3.6 Conclusion

In summary, a fast evaluation method in the form of empirical equations for the quick estimation of natural ventilation and energy saving potential was developed with multiple parameters taken into account, such as building location, terrain, opening size and orientation, etc. The relation between the wind incidence angle and the two coefficients f and ΔC_p was studied and discussed. The model validation, sensitivity study and continuity verification proved the credibility of the simulation.

This fast evaluation approach was turned into an Excel-VBA-based natural ventilation evaluation tool which could be widely used to evaluate the viability of natural ventilation to save energy during early building designs. By setting the necessary parameters, architects and engineers could have access to direct impressions of natural ventilation performance and be able to make their own judgments quickly.

However, in reality, natural ventilation performance can be significantly affected by many factors such as the surrounding environment, the internal layout of the building and the location of the openings. In future studies, we are interested in developing a map of natural ventilation potential for North America to determine more possible tendencies and study natural ventilation under both wind- and buoyancy-driven conditions, which is more practical for real buildings and particularly high-rise buildings.

4 Hybrid Ventilation Study for Predictive Control

4.1 Problem statements

As one of the effective measures to reduce cooling energy consumption, hybrid ventilation combines the benefits of natural and mechanical ventilation and it could reduce cooling load significantly when it is used with proper control strategy [71], [72]. Many previous studies have been conducted on hybrid ventilation systems by carrying out on-site measurements under one specific or different control strategies [68], [73] and [74].

Most of these previous researches focused on single houses or low-rise buildings and a full-scale hybrid ventilation study, especially on-site measurements in actual high-rise buildings, is rather limited. As reviewed in previous chapter, although the IEA EBC Annex 62 [5] includes a series of different buildings, there is still a lack of whole-building and full-scale data for high-rise buildings with hybrid ventilation. On the other hand, a high-rise building often consumes more energy than low-rises, and its mechanical system is more complex. It is still a challenge how to optimally operate a high-rise hybrid ventilation system under variable weather conditions while keeping acceptable comfort conditions.

Predictive controls based on simulation models, i.e. model predictive controls (MPC), have been shown to be very effective to ensure the performance of a hybrid ventilation system, especially under a variable ambient environment [75]. However, it is not practical to use a detailed model of considering all the complexities of the building including its interior structure, thermal mass, mechanical system, cooling/heating loads, and weather conditions, for implementing MPC in a real building (so-called on-line MPC), because MPC often requires certain level of simplifications of the building so it can be easily implemented and used for on-line controls. Therefore, there is a

need for research to develop a relatively simple and practical model for MPC that can easily be calibrated, while capturing the essential airflow and thermal physics of hybrid ventilation at an adequate level for achieving its on-line operations.

4.2 Methodology

To address the research needs, this study presents a full-scale measurement study in a 17-story institutional high-rise building (i.e. EV building) with hybrid ventilation system [43], [76], and a simple hybrid ventilation model based on the method of multizone airflow network. Measurements including mechanical fan flow rates, ambient temperatures and wind conditions, natural ventilation rates at different floors were conducted for two different days. In the present study, the building was first simulated by a detailed 15-zone multizone model using CONTAM, one of the most popular programs to model ventilation for different types of buildings [77]–[79]. The detailed model includes 5 stacked 3-story atriums and defines each floor as one zone exclude the 1st floor and 17th floor that do not have inlets. Based on the detailed model, a simplified 5-zone model is developed and validated by comparing the results to those of the detailed model and the measurement data. An example of using the simplified model is then illustrated for the optimization of the hybrid ventilation of the full-size building.

4.3 Full-scale measurements

The measurements were conducted in a 17-story institutional high-rise building located at the downtown Montreal, Canada (45.5°N, 74°W). The building is with two main large facades facing approximately southwest and southeast respectively. The total floor area is about 53,000 m^2. The

hybrid ventilation system in the building comprises five vertically-stacked atriums, inlet motorized dampers at both ends of the corridor at each floor, and variable speed mechanical fans at the roof (Figure 4-1). The five atriums in the buildings are from the second to the sixteenth floor, spanning three floors each (note: floor 17 is the mechanical room). They are separated with a floor slab and connected with 4-m^2 floor grilles with motorized dampers. The dimensions of each atrium are 9 m (W) × 12 m (L) × 12 m (H). The atrium is used as a solar chimney in the hybrid ventilation mode [41]. The area of the inlet dampers is about 1.4 m^2 when fully opened but can be adjusted by motors.

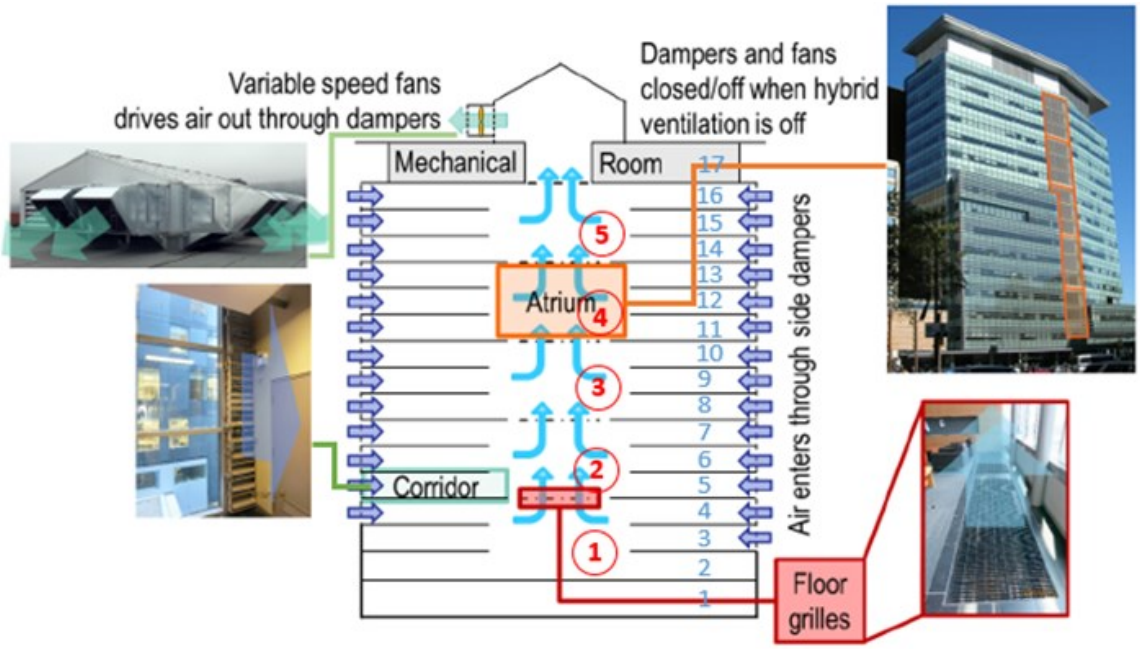

Figure 4-1. Schematic of hybrid ventilation system in a 17-story institutional high-rise building [8]

The measurements were conducted on two different days (See detailed measurement results in Appendix A). Weather conditions, including wind speed and direction, and outdoor temperature, were measured by a weather station at the roof (Table 4-1). Though the outdoor temperature was as low as less than 2 °C in Day 1 (Nov 18th,2015), the cool air was warmed as it flows deeper into

the building due to mixing with the indoor environment, and was around 22°C at the atriums. Since there were few occupants near the inlets, no complaints were reported. Note that due to the different weather conditions and potentially different stack effects, the airflow rate of the roof fans are different even at the same fan frequency, e.g. 40% fan frequency in Day 1 and Day 2 (Nov 8th,2016). Except the fan frequency, all the other data are averaged over time. Table 4-2 shows the opening area percentage of the inlet dampers for natural ventilation: they were fully open on Day 1 but closed for the floors 2, 3, 14-16 on Day 2.

Table 4-1. Measurement conditions.

Day	**Roof fan frequency (%)**	**Roof fan flow rate (L/s)**	**Outdoor temperature (°C)**	**Wind speed (m/s)**
Day 1	20	17291	1.45	3.55
	40	24325	1.70	2.84
	60	31810	1.35	1.54
	80	36707	1.85	1.21
Day 2	40	18117	14.64	1.80

Table 4-2. Inlet dampers opening percentage.

Floor section	**1**	**2**	**3**	**4**	**5**
Day 1	100%	100%	100%	100%	100%
Day 2*	90%	40%	65%	100%	/

* Dampers on floors 2, 3, 14-16 were closed.

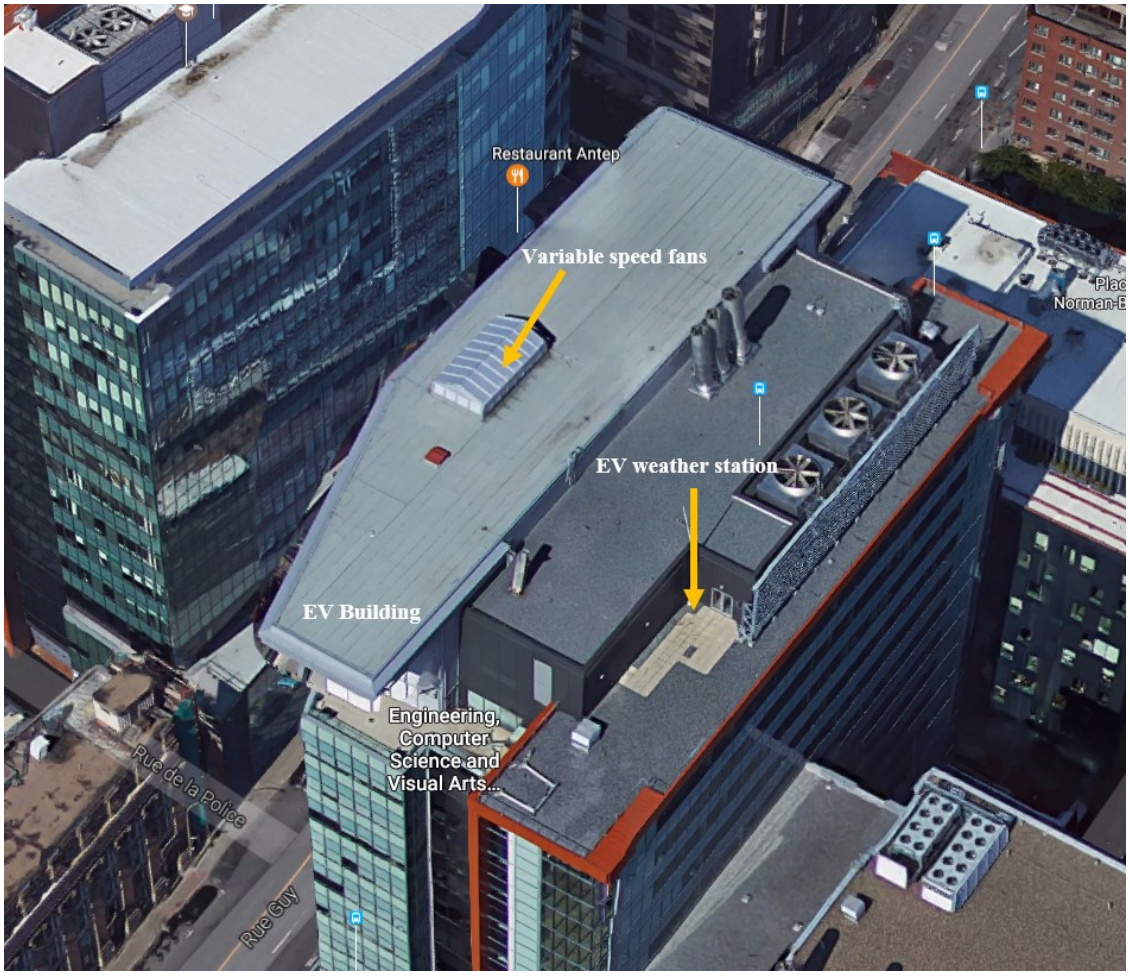

Figure 4-2. Weather station and variable speed fans location.

Natural ventilation velocities near the inlet dampers were measured by hot-wire anemometers with sampling time of 60 seconds, and collected by a data logger (Omega HHF-SD1) as shown in Figure 4-3. The measurement range of the air speed is 0.2 ~ 25 m/s and the accuracy is ± (5%+0.1 m/s). The velocity was measured only for the 5th floor on Day 1 and for the 5th, 8th and 11th floors on Day 2. The velocity measurements were then used to calculate mass flow rates through the inlet damper based on their effective opening areas.

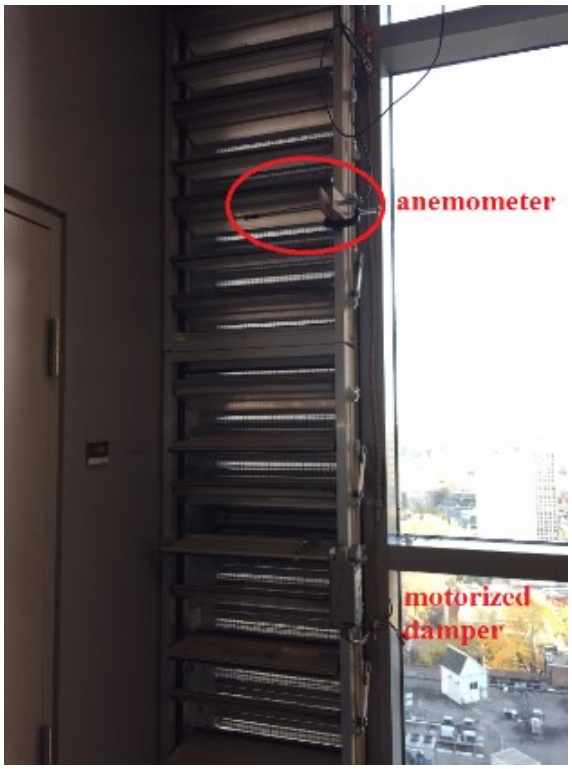

Figure 4-3. Natural ventilation velocity measurement near inlet dampers.

4.4 Simulation

Figure 4-4 shows a schematic of the detailed simulation model in CONTAM, which includes all corridors, dampers, offices, atriums, stairwells and elevator shafts. Since this detailed model was based on the floors, there is a total of 15 sections (1st floor and 17th floor are not included since they do not have inlets). Based on the number of atrium sections, a simplified model is developed to model each atrium as one zone, so there are five zones for the simplified model, i.e. the so-called 5-zone model.

Mass flow rate through each inlet damper is one of the key parameters for a hybrid ventilation system because it indicates the amount of free cooling available from natural ventilation. In CONTAM, it is modeled by Eq. 4-1, the power-law flow model [80], with the flow exponent, n = 0.5 in this study. $\dot{m}$ is the mass flow rate in kg/s; ρ_0 is the outdoor air density, kg/m^3; Δp is the pressure difference across the damper, Pa; C is the flow coefficient, m^2. The flow coefficient, C, was calibrated by comparing the simulated and measured mass flow rates for the tests on both days.

$$\dot{m} = C\sqrt{\rho_0}(\Delta p)^n \qquad \text{Eq. 4-1}$$

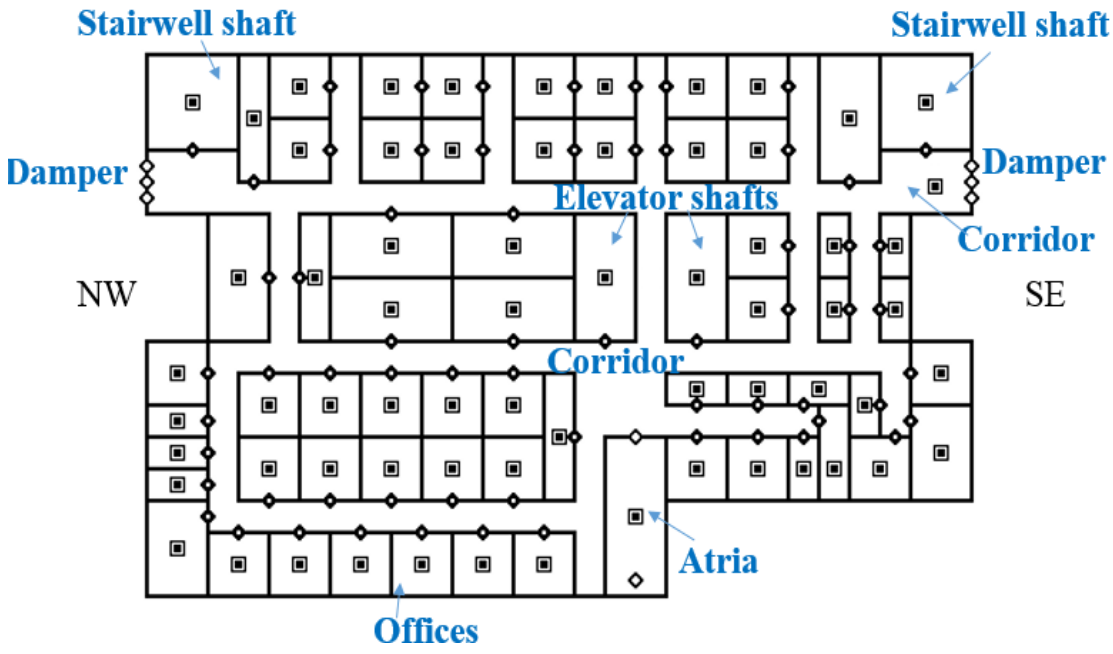

Figure 4-4. The detailed CONTAM simulation model.

4.5 Results

By definition, the value of the flow coefficient, C, is empirical and variable with different weather conditions. In this study, the flow coefficients were calibrated and obtained for both days of tests.

In this section, the results of the calibration are first presented for both Day 1 and 2, and followed by a comparison study of the detailed model and the simplified 5-zone model for Day 1.

4.5.1 Simplified model calibration in Day 1

In Day 1, the inlet damper velocity at the 5th floor was monitored under different desired flow rate settings (frequency setting of the variable speed drive) of the roof fan. Figure 4-5 compares the corresponding inlet natural ventilation flow rates between the measurements and the simulations after calibrations. The calibrated flow coefficient, *C*, for the simplified model varies between 0.57 and 0.64 with an average value of 0.62 for all fan frequencies.

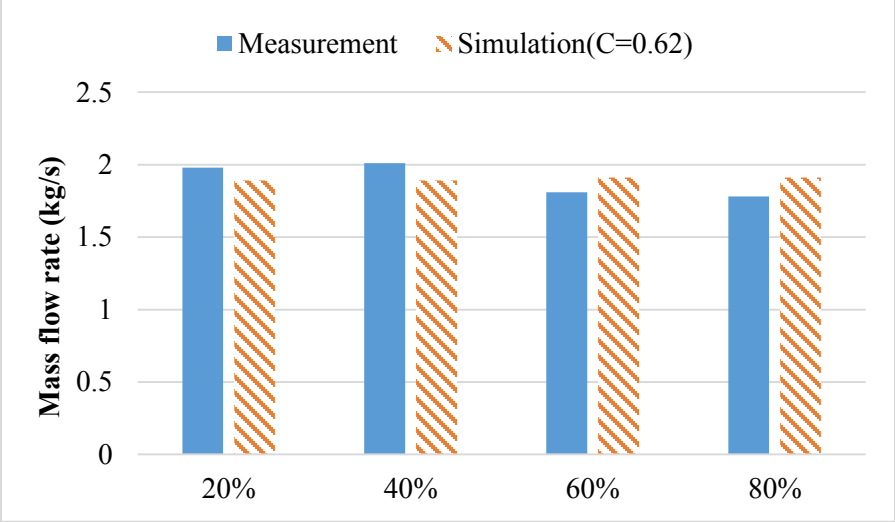

Figure 4-5. Inlet damper flow rate at the 5th floor for different roof fan frequencies (20% ~ 80%) and corresponding flow coefficients after calibration (Day 1)

With the average flow coefficient, the predicted mass flow rates through the inlet damper at the 5th floor were compared to the measured data in Table 4-3. The relative difference is within 4% and 7%.

Table 4-3. Predicted and measured mass flow rates through the damper at the 5th floor for different frequencies of the roof fan.

VFD of roof fan	20%	40%	60%	80%
Measured data (kg/s)	1.98	2.01	1.81	1.78
Predicted result (kg/s)	1.89	1.89	1.91	1.91
Relative difference	4.5%	6.3%	4%	7%

4.5.2 Simplified model calibration in Day 2

With the average value of coefficient, $C = 0.62$, obtained from the calibration on Day 1, we simulated the whole building for Day 2. Figure 4-6 shows that there exists a significant discrepancy of up to 80% between the simulation results and the measurements. Therefore, the flow coefficient needs to be re-calibrated for the new weather and operating conditions for Day 2. The values of C of the inlet dampers were thus adjusted for each atrium section as shown in Table 4-4. After the re-calibration, Figure 4-6 shows that the simulated flow rates at the 5^{th}, 8^{th}, and 11^{th} floors were more uniform, and closer to the measured data than before the calibration. To be specific, the difference between the simulation results and the measurements is reduced greatly, it varies from 0% to maximally 30% in different floors of building.

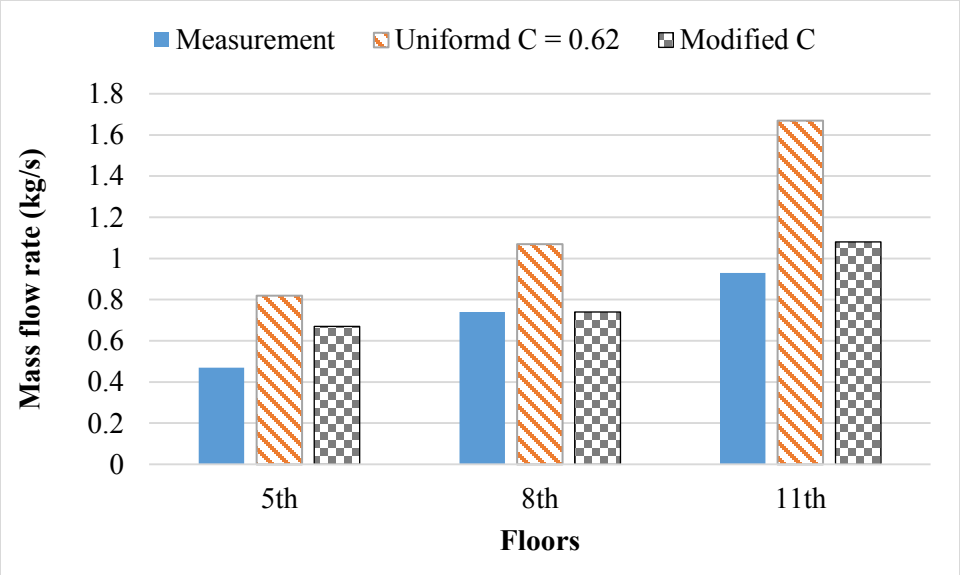

Figure 4-6. Inlet damper flow rates at different floors and the calibrations of the flow coefficients (Day 2).

Table 4-4. Modified value of flow coefficients, C, in the detailed CONTAM model (Day 2).

Section	**1**	**2**	**3**	**4**
Floor	4	5-7	8-10	11-13
Value of *C*	1.11	0.15	0.19	0.28

Table 4-5. Predicted and measured mass flow rates through the damper at the different floors for 40% frequency of the roof fan.

Floor number	5th	8th	11th
Measured data (kg/s)	0.47	0.74	0.93
Predicted result (kg/s)	0.67	0.74	1.08
Relative difference	29.8%	0%	13.9%

4.5.3 Comparison between detailed model and simplified model

Figure 4-7 compares the simulation results of the detailed and simplified models. Normalized root-mean-square deviation (NRMSE) is used here to quantify the difference between the two models Eq. 4-2 [81]. $\dot{m}_{d,i}$ and $\dot{m}_{s,i}$ are the mass flow rates through the damper at i^{th} floor for the detailed model and simplified model. N is the total number of the sections modeled. A smaller value of NRMSE indicates that the results of the simplified model are closer to the detailed model. In this study, the calculated NRMSE is 0.014, showing that the results of the two models are very close. Therefore, the simplified model can be used to replace the detailed model as the hybrid ventilation model for the building's predictive control of the inlet damper openings in each atrium based on anticipated/predicted weather conditions.

$$NRMSE = \frac{\left[\frac{1}{N}\sum_{i=2}^{N}\left(\dot{m}_{d,i} - \dot{m}_{s,i}\right)^2\right]^{\frac{1}{2}}}{\dot{m}_{d,\max} - \dot{m}_{d,\min}} \qquad \text{Eq. 4-2}$$

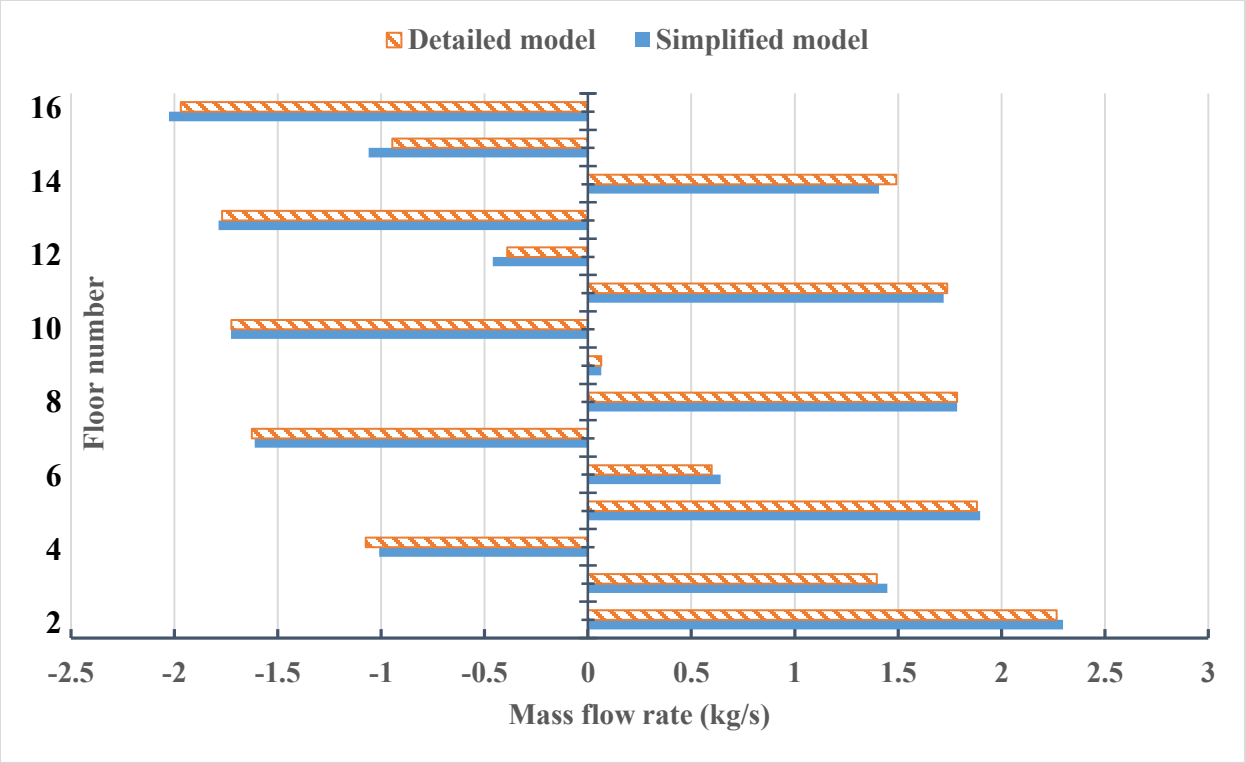

Figure 4-7. The comparison of predicted flow rates at the inlet dampers between the detailed and simplified models.

4.6 Discussion

To demonstrate the simplified model for potential use for predictive control applications, an example was used here for achieving evenly distributed natural ventilation flows through all the inlet dampers at different floors so as to naturally cool all 15 floors. This is realized by adjusting the damper opening areas.

Figure 4-8 presents the flow rates under the weather conditions of Day 1 for the fan frequency of 40% (i.e. desired flow rate about 40% of maximum). It shows that the flow rate is quite non-uniform when all the dampers are fully opened. The flow rates of the 1st, 2nd and 5th sections are much larger than the middle sections. In order to make all floors equally benefit from the natural

cooling, it is preferred to distribute the inlet flow rates evenly by adjusting the damper opening sizes: reduce the opening percentage of the 1st, 2nd, and 5th sections as shown in Table 4-6.

The effect of the optimization can be shown by quantifying a non-uniformity factor of the flow rate, the non-uniformity coefficient, k, as defined by Eq. 4-3 [82]. Here, $\overline{\dot{m}}$ is the average flow rate through the dampers at different floors; N is the total number of the sections modeled. A better uniformity of the flow among all inlet dampers means a smaller value of k. It is found that the value of k drops significantly from 0.74 before the optimization to 0.06 after the dampers opening sizes are adjusted. Therefore, the optimization of the damper opening area is an effective approach to achieve uniform natural ventilation flow among dampers at different floors.

$$k = \frac{\sigma}{\overline{\dot{m}}} \qquad \text{Eq. 4-3}$$

$$\text{where } \sigma = \sqrt{\frac{\sum\left(\dot{m}_i - \overline{\dot{m}}\right)}{N}}$$

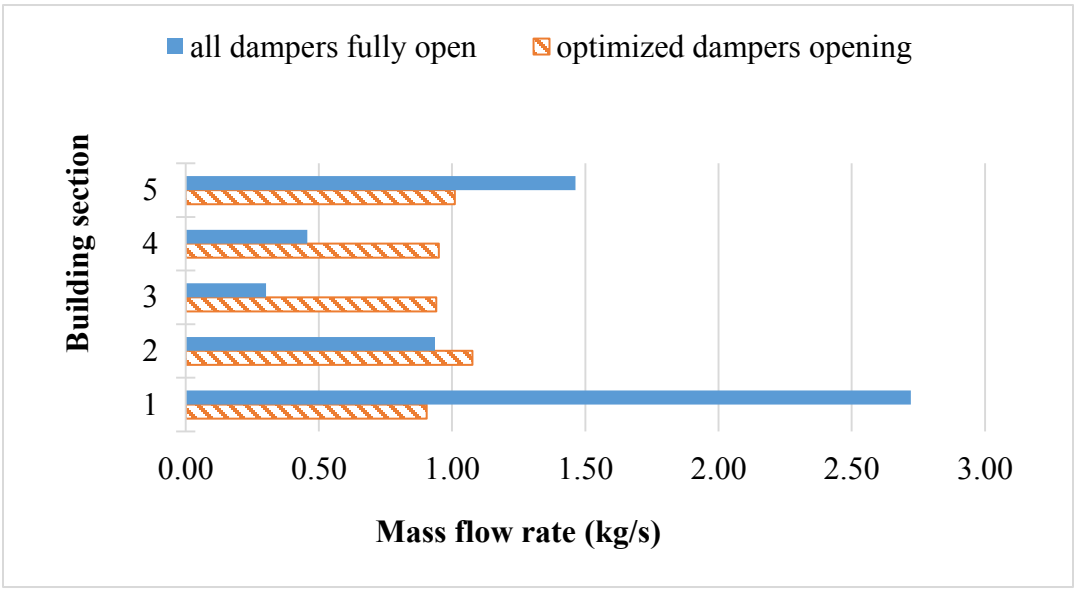

Figure 4-8. Comparing the natural ventilation inlet flow rates when all dampers are fully opened and when the damper openness are adjusted for achieving better uniformity at fan frequency 40% (Day 1).

Table 4-6. Damper opening percentage after the optimization.

Section	**1**	**2**	**3**	**4**	**5**
Floor	3	5-7	8-10	11-13	14-16
Day 1	15%	45%	100%	100%	40%

4.7 Conclusion

This chapter reports a series of full-scale measurements of hybrid ventilation in a 17-story institutional building and associated whole-building simulations using both a 15-zone detailed and a 5-zone simplified multizone models. Full-scale measurements were conducted in two different days with significantly different ambient weather conditions. Mechanical fan flow rates at different fan frequencies, mass flow rates through dampers at different floors, outdoor temperature and wind conditions were measured. The simplified model of the whole building was calibrated by the measured data for both days. The simulated results were also compared to a detailed model of the building using CONTAM. To illustrate the optimization of the high-rise hybrid ventilation system using the simplified model, an example was also provided.

This study shares many important experiences of full-size high-rise building measurements and whole-building simulations. For example, it is found that the variations of weather conditions and their dynamic interactions with hybrid ventilation systems can be accounted for by flow coefficients in the simplified model of the building. Although the simplified model only needs five zones, the difference of the predictions between the detailed and simplified models is within 10%, indicating that it is possible to model the whole building in a simple way for the future on-line model-predictive control (MPC) applications of this high-rise building. The demo case study in

the discussion section shows that the optimization of the damper opening area is an effective approach to achieve uniform natural ventilation flow through dampers at different floors.

Future studies are needed to implement the simplified model for actual on-line MPC applications of the building. The simplified model will also be further developed to include energy balance calculations for thermal mass analysis for future MPC applications of thermal storage for the building. More measurements are expected in 2017 to collect more data under different weather conditions, which will be used for the further analysis of hybrid ventilation systems in high-rise buildings and validation of the simplified model with energy balance equation.

5 Conclusions

5.1 Summary and Conclusions

This thesis firstly studied the existing empirical models for the calculation of natural ventilation airflow rates. Two crucial coefficients, f and $\Delta C_{p,}$ which stand for single-sided and cross-ventilation respectively, were researched by conducting CFD simulations in order to determine how the two coefficients would be affected by factors such as wind incidence angle, building height, etc. Both the steady RANS standard two-equation k-ε model and the LES model were used in the computational simulations. Additionally, the credibility of the simulation was verified via model validation, sensitivity study and continuity verification.

With newly-determined coefficients, a quick and relatively accurate evaluation method was developed in the form of empirical equations for the estimation of natural ventilation energy saving potential by considering multiple parameters such as building location, terrain, opening size and orientation. According to the Toronto case study, a building with a window-to-wall ratio of 30% has around 5% more natural ventilation energy saving potential than buildings with a window-to-wall ratio of 40% under both ventilation strategies, i.e. single-sided and cross-ventilation. Sliding windows were found to have up to 10% more natural ventilation energy saving potential than casement and tilt windows when other parameters were kept constant. Natural ventilation could also be used to save energy during transition season and winter, especially, in buildings with high internal heat gain such as high-tech offices or data centers, which are more suitable with relatively lower summer and higher winter average daily temperatures to maximize energy savings from natural ventilation.

This thesis also illustrates research towards optimizing hybrid ventilation performance in a 17-story institutional building, i.e. the Concordia University EV building. A series of on-site measurements of inlet air velocity and temperature were conducted under different conditions to compare and calibrate the 5-zone simplified CONTAM model. In addition, this 5-zone simplified model was compared with a 15-zone detailed model which showed only minor differences (within 10%), indicating that it is feasible to model the whole building in a relatively simple way for future on-line model-predictive control (MPC) applications in the EV building. Moreover, in such a simplified model, variations in weather conditions and their dynamic interactions with the hybrid ventilation systems can be accounted for by flow coefficients. A demo case study showed that hybrid ventilation performance can be optimized by adjusting the damper opening area, achieving uniform natural ventilation flow through dampers on different floors of the building.

5.2 Contributions

An Excel-VBA tool is developed to estimate natural ventilation energy saving potential based on the empirical equations formed fast evaluation method. This tool can be used by engineers and architects under different:

- Ventilation strategies (single-sided or cross ventilation)
- Building locations (city and terrain)
- Building details (floor area, number of floors, etc.)
- Opening details (window-to-wall ratio and window type)
- Indoor design temperature range
- Internal heat gains

A five-zone simplified model is conducted that is capable of studying the performance of hybrid ventilation system in EV building, Concordia University. This model can be used to simulate different weather conditions, exhaust fan operating conditions (i.e. exhaust flow rate and working frequency) and inlet damper opening areas.

5.3 Future work

It would be interesting to generate a Graphics Processing Unit (GPU)-based rendering map of natural ventilation energy saving potential in North America (see Figure 5.1) based on public weather files, not only to explore possible existing tendencies, but also to render the Excel-VBA-based evaluation tool fully functional and less time consuming for use by architects and engineers by being able to provide intuitive impressions of natural ventilation energy saving potential during the building's conceptual design stage. Specifically, besides showing the annual hour of natural ventilation potential and annual possible energy saving (in kWh) by natural ventilation, this map would also be capable of presenting the optimum range of internal heat gain for North American buildings, and the energy saving potential would be subdivided into whole day hour and night hour, working hour and weekend hour respectively. Once this GPU-based rendering map is capable of serving North American buildings' natural ventilation energy saving potential, it could be further developed into a worldwide natural ventilation energy saving potential map. Besides wind-driven ventilation, the buoyancy force is more specific and independent to buildings with various internal layout. For example, the existence of solar chimney could improve the ventilation performance significantly. Thus, the force of buoyancy should not be neglected since many existing buildings use the force of buoyancy to enhance ventilation performance.

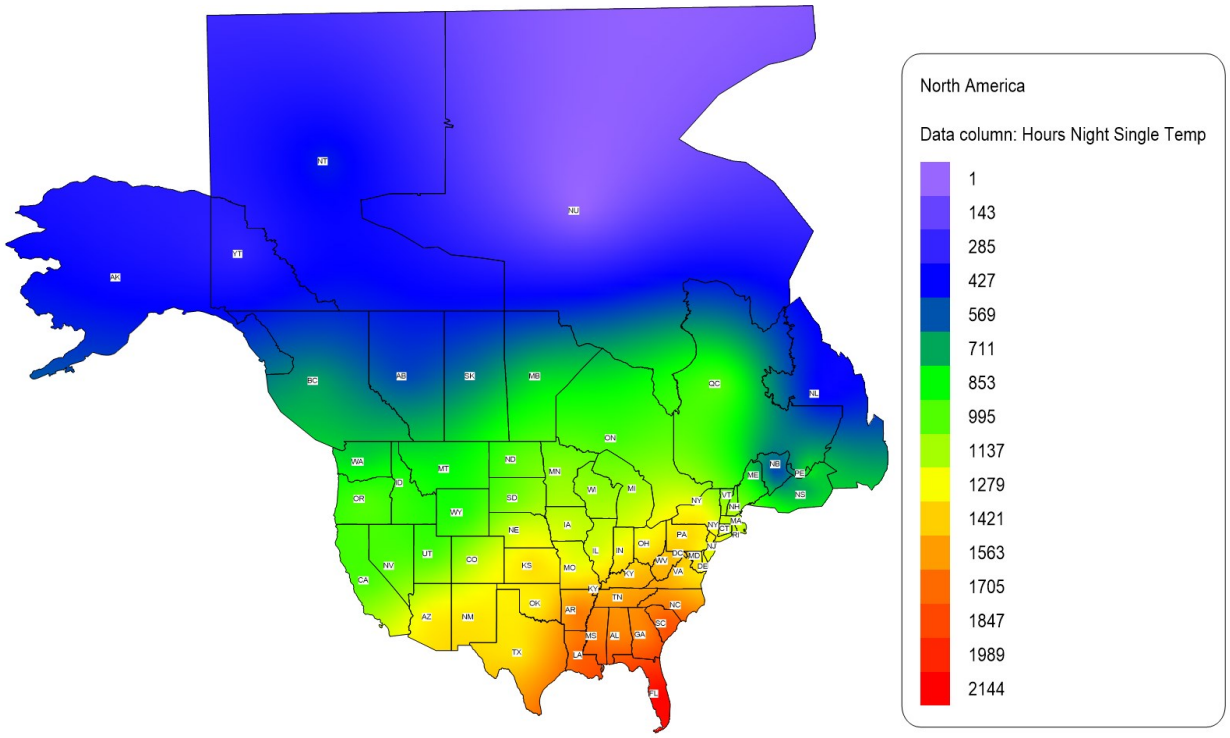

Figure 5-1. Demo North American natural ventilation energy saving potential map (night hour only, single-sided ventilation)

The simplified model also needs to be developed further to combine energy balance calculations for MPC applications in terms of thermal mass analysis. To do so, more full-scale measurements under various weather conditions are required to gather more data. Besides the air temperature in the dampers, also the surface temperature of walls and floor adjacent to the dampers needs to be measured and the temperature change is necessary to be compared with the data of dampers to explore potential links. In addition, small-scale experiments based on the full-scale EV building measurements could be conducted as supplements to validate and calibrate the computational simulations. Eventually, the simplified model needs to be implemented into actual on-line MPC applications of the EV building.

6 References

[1] O. Seppänen and W. J. Fisk, "Association of ventilation system type with SBS symptoms in office workers.," *Indoor Air*, vol. 12, no. 2, pp. 98–112, 2002.

[2] DOE, "2011 Buildings Energy Data Book," 2012.

[3] OEE, "Secondary Energy Use by End-Use," *Off. Energy Effic. Nat. Resour. Canada*, 2011.

[4] Natural Resources Canada, "Energy Use Data Handbook, 1990 to 2010," 2013. [Online]. Available: http://oee.nrcan.gc.ca/publications/statistics/handbook2010/handbook2013.pdf.

[5] Venticool, "IEA EBC Annex 62: The IEA project on ventilative cooling," *EBC*, 2016. [Online]. Available: http://venticool.eu/venticool-home/.

[6] B. Krausse, M. Cook, and K. Lomas, "Environmental performance of a naturally ventilated city centre library," *Energy Build.*, vol. 39, no. 7, pp. 792–801, 2007.

[7] M. Jicha and P. Charvat, "Hybrid ventilation Guidelines," pp. 1–6, 2007.

[8] S. Yuan, "A Study of Hybrid Ventilation in an Institutional Building for Predictive Control," Master thesis, Concordia University, 2016.

[9] J. Bruhn, W. Fry, and G. Fick, "Simulation of daily weather data using theoretical probability distributions.," *J. Appl. Meteorol.*, vol. 19, no. 9, pp. 1029–1036, 1980.

[10] E. Wang, Y. Zhang, J. Luo, F. H. S. Chiew, and Q. J. Wang, "Monthly and seasonal streamflow forecasts using rainfall-runoff modeling and historical weather data," *Water Resour. Res.*, vol. 47, no. 5, 2011.

[11] D. B. Crawley and Y. J. Huang, "Does it matter which weather data you use in energy simulations," *Build. Energy Simul. User News*, vol. 18, no. 1, pp. 25–31, 1997.

[12] L. Buckley, "New - Trend Natural Ventilation Potential & Analytics for Various Climates in Canada," in *eSim 2014*, 2014.

[13] "EnergyPlus weather files." [Online]. Available: https://energyplus.net/weather.

[14] D. B. Crawley and L. K. Lawrie, "Rethinking the TMY: Is the 'typical' meteorological year best for building performance simulation?," in *Proceedings of BS*, 2015, pp. 2655–2662.

[15] T. S. Larsen, "Natural Ventilation Driven by Wind and Temperature Difference," Phd thesis, Aalborg University, 2006.

[16] R. Edwards, *Handbook of Domestic Ventilation*. Elsevier Butterworth-Heinemann, 2005.

[17] P. Karava and T. Stathopoulos, "Wind-induced internal pressures in buildings with large

façade openings," *J. Eng. Mech.*, vol. 138, no. 4, pp. 358–370, 2012.

[18] P. Karava, T. Stathopoulos, and A. K. Athienitis, "Wind-induced natural ventilation analysis," *Sol. Energy*, vol. 81, no. 1, pp. 20–30, 2007.

[19] L. Wang, Y. Pan, and Z. Huang, "Factors Affecting Discharge Coefficient of Building Ventilation Windows (in Chinese)," *Build. Energy Effic.*, vol. 40, no. 6, 2012.

[20] P. Karava, T. Stathopoulos, and A. K. Athienitis, "Wind Driven Flow Through Openings – A Review of Discharge Coefficients," *Int. J. Vent.*, vol. 3, no. 3, pp. 255–266, 2004.

[21] ASHRAE (American Society of Heating Refrigerating and Air-Conditioning Engineers), *2013 ASHRAE Handbook - Fundamentals*. 2013.

[22] G. S. Brager and R. De Dear, "A standard for natural ventilation," *ASHRAE J.*, vol. 42, no. 10, pp. 21–28, 2000.

[23] A. Farghal and A. Wagner, "Studying the Adaptive Comfort Model a Case Study in a Hot Dry Climate , Cairo, Egypt," *Adapt. to Chang. New Think. Comf. Cumberl.*, no. April, pp. 9–11, 2010.

[24] R. J. de Dear, "A global database of thermal comfort field experiments," *ASHRAE Trans.*, vol. 104, no. 1b, pp. 1141–1152, 1998.

[25] H. Feriadi, "Thermal comfort for naturally ventilated residential buildings in tropical climate," National University of Singapore, 2004.

[26] X. J. Ye, Z. P. Zhou, Z. W. Lian, H. M. Liu, C. Z. Li, and Y. M. Liu, "Field study of a thermal environment and adaptive model in Shanghai," *Indoor Air*, vol. 16, no. 4, pp. 320–326, 2006.

[27] A. Farghal and A. Wagner, "Studying the Adaptive Comfort Model a Case Study in a Hot Dry Climate , Cairo, Egypt," *Adapt. to Chang. New Think. Comf. Cumberl.*, no. April, pp. 9–11, 2010.

[28] P. R. Warren, "Ventilation through openings on one wall only," in *Energy conservation in heating, cooling and ventilating buildings*, 1977, vol. 1, pp. 189–209.

[29] P. R. Warren and L. M. Parkins, "Single-sided ventilation through open windows," in *Conf. proc. Thermal Performance of the Exterior Envelopes of Buildings, ASHRAE, Florida*, 1985, vol. 49, p. 20.

[30] R. D. Crommelin and E. M. H. Vrins, "Ventilation through a single opening in a scale model," *Air Infiltration Rev.*, vol. 9, no. 3, pp. 11–15, 1988.

[31] H. Wang and Q. Chen, "A new empirical model for predicting single-sided, wind-driven

natural ventilation in buildings," *Energy Build.*, vol. 54, pp. 386–394, 2012.

[32] J. P. Cockroft and P. Robertson, "Ventilation of an enclosure through a single opening," *Build. Environ.*, vol. 11, no. 1, pp. 29–35, 1976.

[33] W. de Gids and H. Phaff, "Ventilation rates and energy consumption due to open windows. A brief overview of research in the Netherlands," *Air Infiltration Rev.*, vol. 4, no. 1, pp. 4–5, 1982.

[34] F. Allard and M. Santamouris, "Natural ventilation in buildings: a design handbook," in *London James James*, 1998, p. 378.

[35] D. W. Etheridge and M. Sandberg, *Building ventilation: theory and measurement*. 1996.

[36] P. Heiselberg, "Natural and Hybrid Ventilation," Noteslecture notes from the PhD-course Modelling natural and hybrid ventilation, Aalborg University, 2005.

[37] C. Allocca, Q. Chen, and L. R. Glicksman, "Design analysis of single-sided natural ventilation," *Energy Build.*, vol. 35, no. 8, pp. 785–795, 2003.

[38] D. W. Etheridge and M. Sandberg, *Building ventilation: theory and measurement*. 1996.

[39] BUILDING ADVENT, "Advanced Ventilation Technologies, Case Study No.4." [Online]. Available: http://portal.tee.gr/portal/page/portal/INTER_RELATIONS/english/UIA-ARES/PROGRAMS/73B07C33CD6BE3C7E04046D412C204D6.

[40] BUILDING ADVENT, "Advanced Ventilation Technologies, Case Study No.8." [Online]. Available: http://portal.tee.gr/portal/page/portal/INTER_RELATIONS/english/UIA-ARES/PROGRAMS/73B084CD78B645A9E04046D413C237E7.

[41] A. Tzempelikos, A. K. Athienitis, and P. Karava, "Simulation of facade and envelope design options for a new institutional building," *Sol. Energy*, vol. 81, no. 9, pp. 1088–1103, 2007.

[42] E. Mouriki, P. Karava, A. K. Athienitis, K.-W. Park, and T. Stathopoulos, "Full-Scale Study of an Atrium Integrated With a Hybrid Ventilation System," in *4th Canadian solar buildings conference*, 2009, no. 2, pp. 2–9.

[43] P. Karava, A. K. Athienitis, T. Stathopoulos, and E. Mouriki, "Experimental study of the thermal performance of a large institutional building with mixed-mode cooling and hybrid ventilation," *Build. Environ.*, vol. 57, pp. 313–326, 2012.

[44] M. V. Swami and S. Chandra, "Correlations for pressure distribution on buildings and calculation of natural-ventilation airflow," *ASHRAE Trans.*, vol. 94, no. 1, pp. 243–266, 1988.

[45] M. W. Liddament, "A guide to energy efficient ventilation," *Air Infilteration Vent. Center,*

(AIVC)., p. 252, 1996.

[46] P. Karava, T. Stathopoulos, and A. K. Athienitis, "Impact of internal pressure coefficients on wind-driven ventilation analysis," *Int. J. Vent.*, vol. 5, no. 1, pp. 53–66, 2006.

[47] K. . Andersen, P. Heiselberg, and S. Aggerholm, "Naturlig ventilation i erhvervsbygninger (in Danish)," *Statens byggeforskningsinstitut*, 2002.

[48] T. van Hooff, B. Blocken, L. Aanen, and B. Bronsema, "A venturi-shaped roof for wind-induced natural ventilation of buildings: Wind tunnel and CFD evaluation of different design configurations," *Build. Environ.*, vol. 46, no. 9, pp. 1797–1807, 2011.

[49] J. K. Calautit and B. R. Hughes, "Wind tunnel and CFD study of the natural ventilation performance ofa commercial multi-directional wind tower," *Build. Environ.*, vol. 80, pp. 71–83, 2014.

[50] J. O. P. Cheung and C. H. Liu, "CFD simulations of natural ventilation behaviour in high-rise buildings in regular and staggered arrangements at various spacings," *Energy Build.*, vol. 43, no. 5, pp. 1149–1158, 2011.

[51] T. G. Farea, D. R. Ossen, S. Alkaff, and H. Kotani, "CFD modeling for natural ventilation in a lightwell connected to outdoor through horizontal voids," *Energy Build.*, vol. 86, pp. 502–513, 2015.

[52] Y. Jiang, D. Alexander, H. Jenkins, R. Arthur, and Q. Chen, "Natural ventilation in buildings: Measurement in a wind tunnel and numerical simulation with large-eddy simulation," *J. Wind Eng. Ind. Aerodyn.*, vol. 91, no. 3, pp. 331–353, 2003.

[53] Y. Jiang and Q. Chen, "Buoyancy-driven single-sided natural ventilation in buildings with large openings," *Int. J. Heat Mass Transf.*, vol. 46, no. 6, pp. 973–988, 2003.

[54] M. Caciolo, P. Stabat, and D. Marchio, "Numerical simulation of single-sided ventilation using RANS and LES and comparison with full-scale experiments," *Build. Environ.*, vol. 50, pp. 202–213, 2012.

[55] G. Evola and V. Popov, "Computational analysis of wind driven natural ventilation in buildings," vol. 38, pp. 491–501, 2006.

[56] P. Gousseau, B. Blocken, T. Stathopoulos, and G. J. F. van Heijst, "CFD simulation of near-field pollutant dispersion on a high-resolution grid: A case study by LES and RANS for a building group in downtown Montreal," *Atmos. Environ.*, vol. 45, no. 2, pp. 428–438, 2011.

[57] X. Shen, G. Zhang, and B. Bjerg, "Comparison of different methods for estimating ventilation rates through wind driven ventilated buildings," *Energy Build.*, vol. 54, pp. 297–

306, 2012.

[58] H. Montazeri and B. Blocken, “CFD simulation of wind-induced pressure coefficients on buildings with and without balconies: Validation and sensitivity analysis,” *Build. Environ.*, vol. 60, pp. 137–149, 2013.

[59] S. Cui, P. Stabat, and D. Marchio, “Numerical simulation of wind-driven natural ventilation: Effects of loggia and facade porosity on air change rate,” *Build. Environ.*, vol. 106, pp. 131–142, 2016.

[60] R. Ramponi and B. Blocken, “CFD simulation of cross-ventilation for a generic isolated building: Impact of computational parameters,” *Build. Environ.*, vol. 53, pp. 34–48, 2012.

[61] RWDI Inc., “Wind tunnel experimental results,” 2015. .

[62] Y. Tominaga, “Flow around a high-rise building using steady and unsteady RANS CFD: Effect of large-scale fluctuations on the velocity statistics,” *J. Wind Eng. Ind. Aerodyn.*, vol. 142, pp. 93–103, 2015.

[63] F. Toja-Silva, C. Peralta, O. Lopez-Garcia, J. Navarro, and I. Cruz, “Roof region dependent wind potential assessment with different RANS turbulence models,” *Jnl. Wind Eng. Ind. Aerodyn.*, vol. 142, pp. 258–271, 2015.

[64] A. Tzempelikos and A. K. Athienitis, “The impact of shading design and control on building cooling and lighting demand,” *Sol. Energy*, vol. 81, no. 3, pp. 369–382, 2007.

[65] M. C. Dubois and Å. Blomsterberg, “Energy saving potential and strategies for electric lighting in future north european, low energy office buildings: A literature review,” *Energy Build.*, vol. 43, no. 10, pp. 2572–2582, 2011.

[66] ASHRAE (American Society of Heating Refrigerating and Air-Conditioning Engineers), “ASHRAE STANDARD 90.1 Energy Standard for Buildings Except Low-Rise Residential Buildings,” *Society*, vol. 8400, pp. 404–636, 2013.

[67] ANSYS Inc., *ANSYS Fluent Theory Guide*. 2014.

[68] ASHRAE 55, *ASHRAE Thermal Comfort Standard*, vol. 55. 2004.

[69] “Example Internal Loads for Different Space Types.” [Online]. Available: https://sustainabilityworkshop.autodesk.com/buildings/equipment-and-lighting-loads.

[70] Chartered Institution of Building Services Engineers (CIBSE), *Guide A: Environmental design*, 8th ed. Norwich: Page Bros. (Norwich) Ltd, 2015.

[71] C. C. Menassa, N. Taylor, and J. Nelson, “Optimizing hybrid ventilation in public spaces of complex buildings - A case study of the Wisconsin Institutes for Discovery,” *Build.*

Environ., vol. 61, pp. 57–68, 2013.

[72] A. Malkawi, B. Yan, Y. Chen, and Z. Tong, "Predicting thermal and energy performance of mixed-mode ventilation using an integrated simulation approach," *Build. Simul.*, vol. 9, no. 3, pp. 335–346, 2016.

[73] H. Brohus, C. Frier, P. Heiselberg, and O. J. Hendriksen, "Measurements of Hybrid Ventilation Performance in an Office Building," *Int. J. Vent.*, vol. 1, no. November, 2003.

[74] W. J. N. Turner and H. B. Awbi, "Experimental investigation into the thermal performance of a residential hybrid ventilation system," *Appl. Therm. Eng.*, vol. 77, pp. 142–152, 2015.

[75] J. Hu and P. Karava, "Model predictive control strategies for buildings with mixed-mode cooling," *Build. Environ.*, vol. 71, pp. 233–244, 2014.

[76] S. Yuan, A. Athienitis, Y. Chen, and J. Rao, "Development of a thermal model for thermal mass coupled with hybrid ventilation in an institutional building," in *eSim 2016 Conference*, 2016, p. 10.

[77] G. N. Walton and W. S. Dols, *CONTAM User Guide and Program Documentation*. Gaithersburg, MD.: National Institute of Standards and Technology, 2013.

[78] D. Qi, L. Wang, and R. Zmeureanu, "Verification of a multizone airflow and energy network model by analytical solutions to Stack driven flows in buildings," in *eSim 2014*, 2014, p. 8.

[79] D. Qi, L. Wang, and R. Zmeureanu, "Modeling smoke movement in Shafts during high-rise fires by a multizone airflow and energy network program," *ASHRAE Trans.*, vol. 121, no. 2, 2015.

[80] W. S. Dols and B. J. Polidoro, *CONTAM User Guide and Program Documentation*. Gaithersburg, MD: National Institute of Standards and Technology, 2015.

[81] D. Qi, L. Wang, and R. Zmeureanu, "The Effects of Non-uniform Temperature Distribution on Neutral Plane Level in Non-adiabatic High-Rise Shafts During Fires," *Fire Technol.*, 2016.

[82] Z. Lian and D. Qi, "Modification for evaluation indexes of air distribution," *J. Chongqing Univ.*, vol. 32, no. 8, pp. 937–942, 2009.

Appendix A: EV Building Measurement Results

The representative measurement results are shown, including the data of wind velocity and outdoor temperature from EV rooftop weather station, VFD fan flow rate and frequency and damper inflow velocity and temperature measured by anemometer.

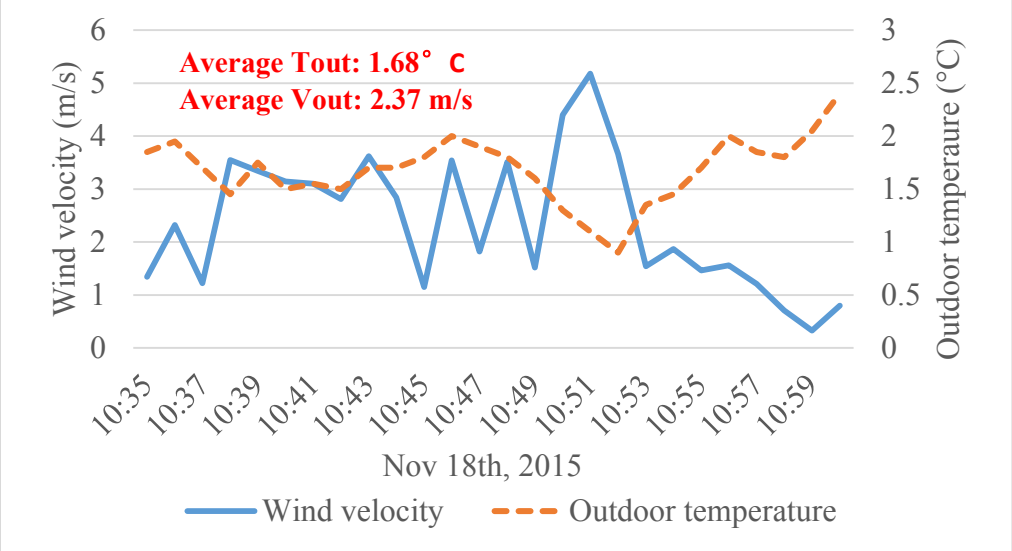

Figure A-1. Wind velocity and outdoor temperature data from rooftop weather station (measurement 1, Nov. 18th 2015)

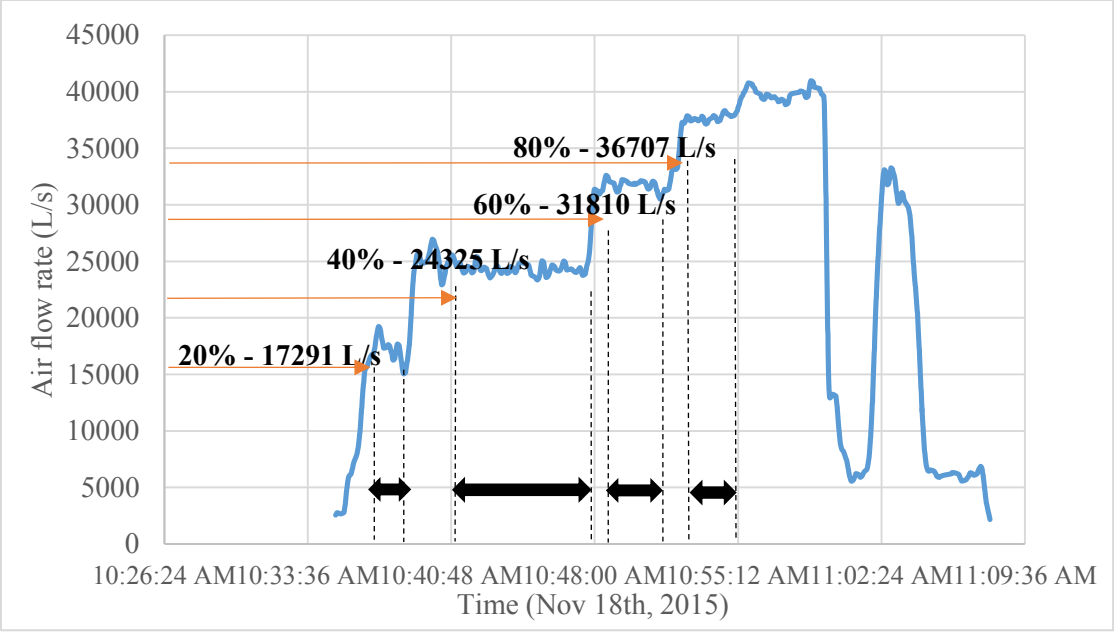

Figure A-2. Average VFD fan flow rates under different frequencies (measurement 1, Nov. 18th 2015)

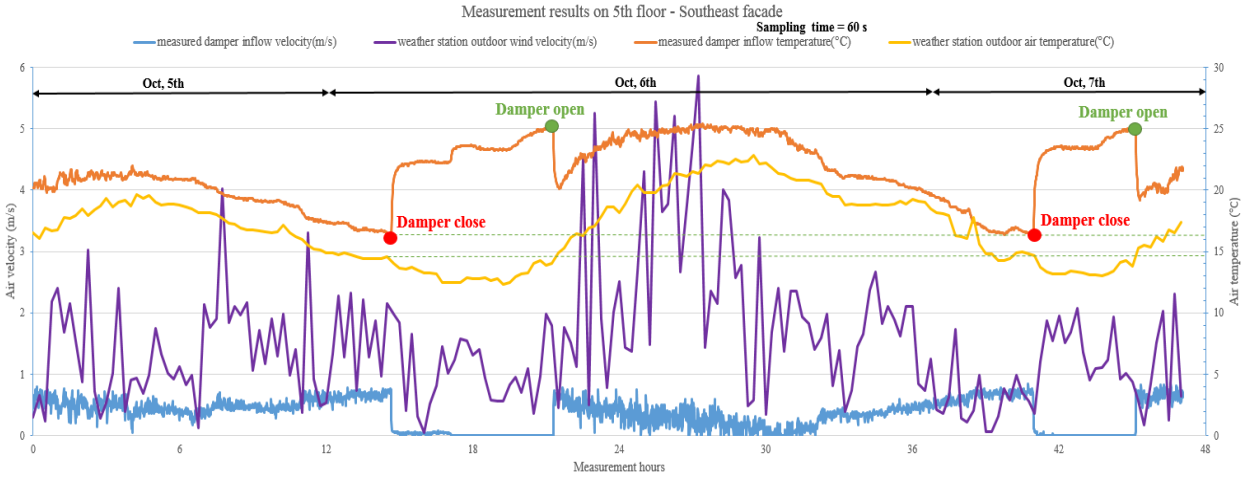

Figure A-3. Measured inflow velocity and temperature on 5th floor southeast facade comparing with wind velocity and outdoor temperature data from rooftop weather station (measurement 2, Oct. 5th 2016)

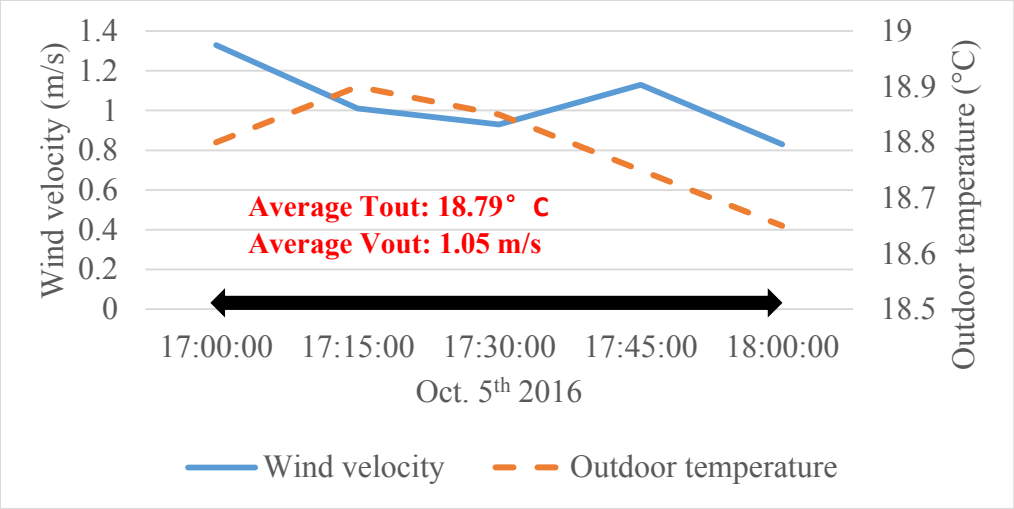

Figure A-4. Average wind velocity and temperature from rooftop weather station used for simulation (measurement 2, Oct. 5th 2016)

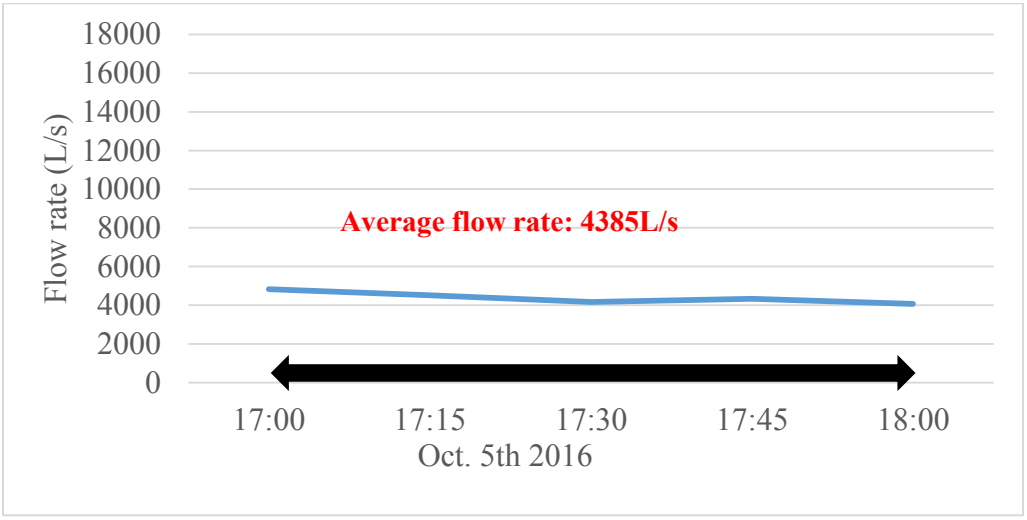

Figure A-5. Average VFD fan flow rate used for simulation (measurement 2, Oct. 5th 2016)

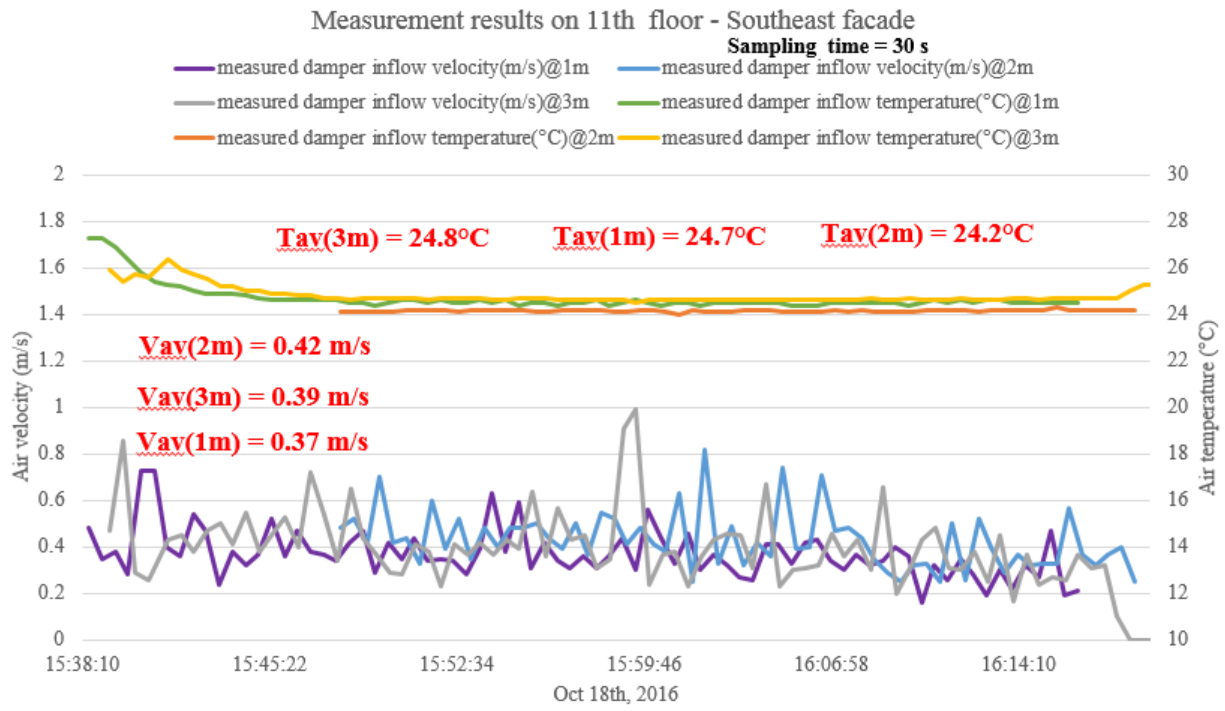

Figure A-6. Measured inflow velocity and temperature on 11th floor southeast facade at three different heights (measurement 3, Oct. 18th 2016)

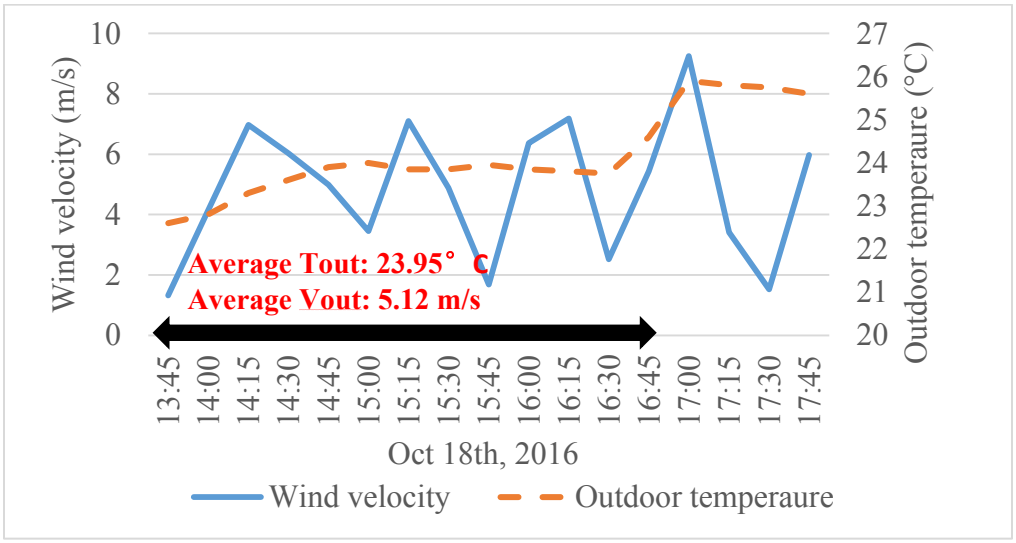

Figure A-7. Average wind velocity and temperature from rooftop weather station used for simulation (measurement 3, Oct. 18th 2016)

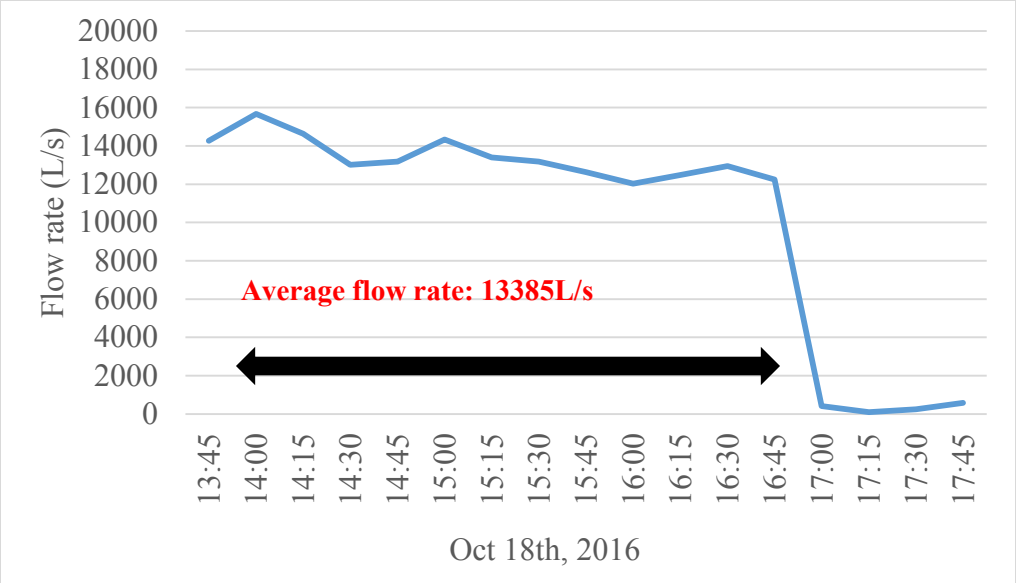

Figure A-8. Average VFD fan flow rate used for simulation (measurement 3, Oct. 18th 2016)

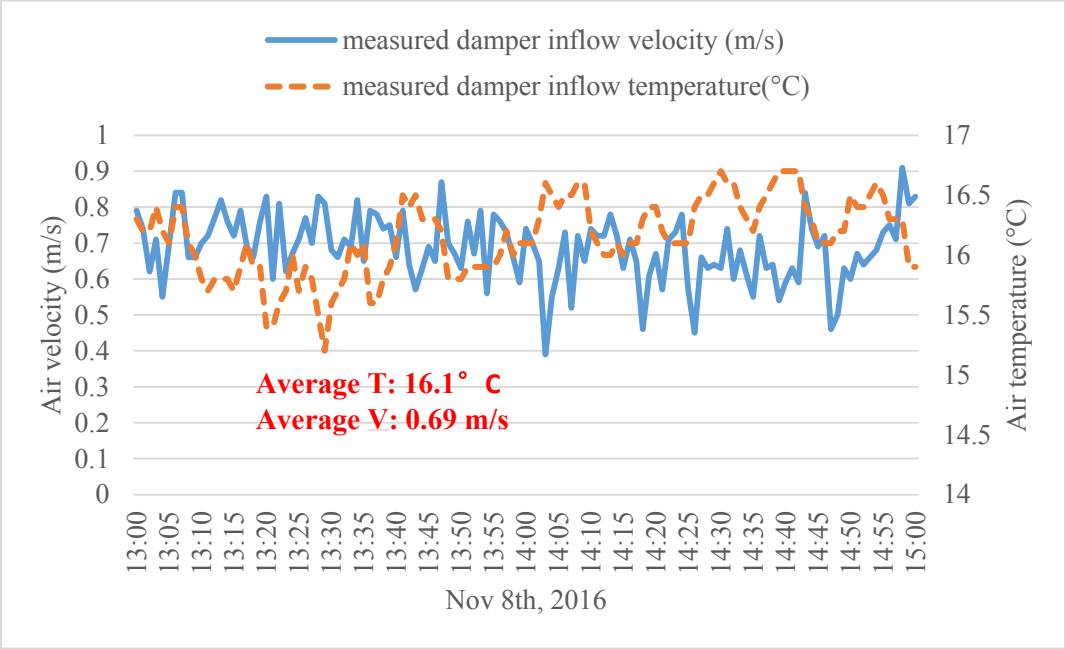

Figure A-9. Measured inflow velocity and temperature on 5th floor southeast facade (measurement 4, Nov. 8th 2016)

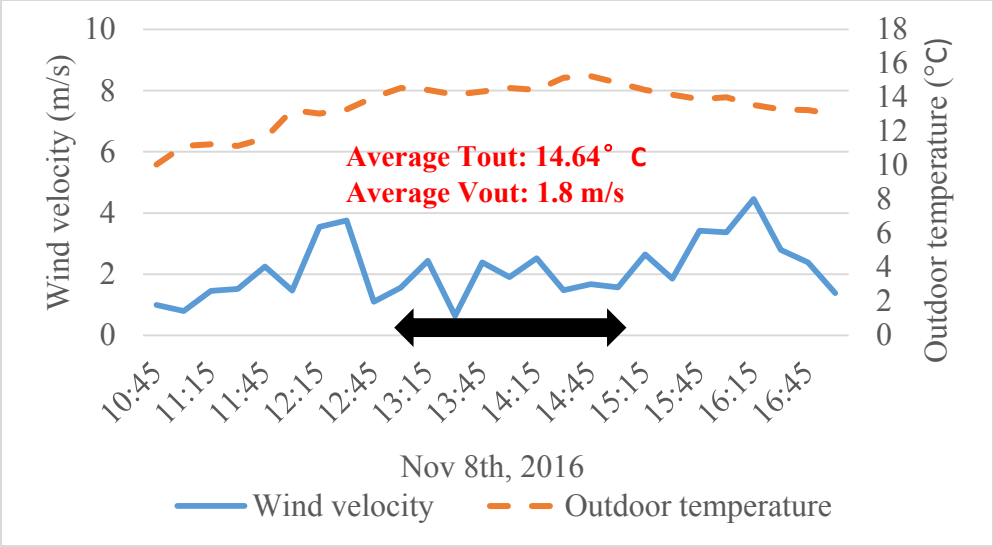

Figure A-10. Average wind velocity and temperature from rooftop weather station used for simulation (measurement 4, Nov. 8th 2016)

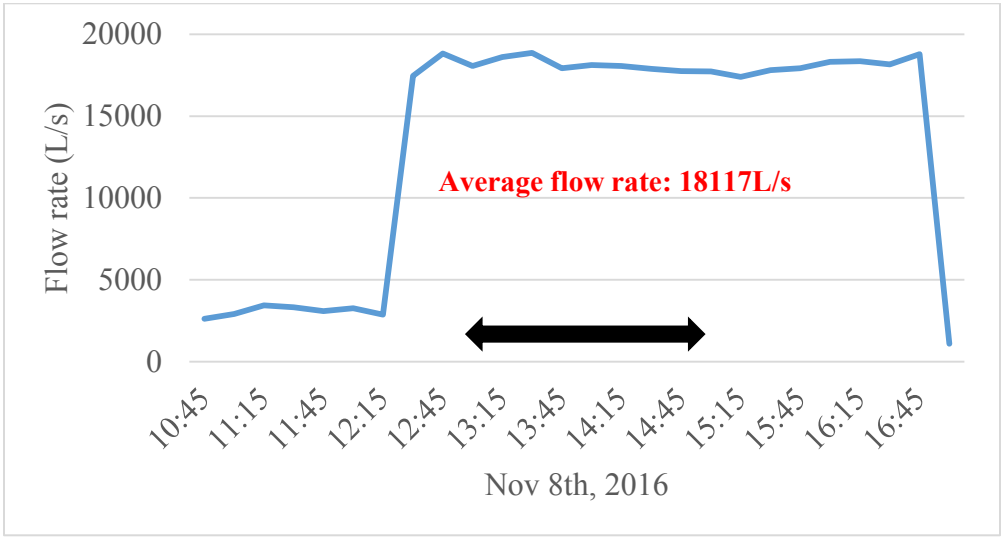

Figure A-11. Average VFD fan flow rate used for simulation (measurement 4, Nov. 8th 2016)